Thermal Spray Processing of Nanoscale Materials II—Extended Abstracts*

C.C. Berndt

The field of nanoscale materials has demonstrated much growth over the last decade. The field of thermal spray has contributed to this growth in terms of powder manufacture, equipment and processing technologies, and the development of coatings and deposits. There is no doubt that thermal spray is a core technology that is underutilized in this emerging area.

This series of conference has been sponsored by The Engineering Foundation, New York, NY, e-mail: engfnd@aol.com, http://www.engfnd.org. The first conference was held in Davos, Switzerland, Aug. 3–8, 1997, and the abstracts published in *JTST*, vol. 7 (3)(1998), pp. 411–41. The second conference, which is reported in this article, was held in Québec City, PQ, Canada, August 15–10. The Conference Co-Chairs were C.C. Berndt (SUNY at Stony Brook), E.J. Lavernia (University of California, Irvine), L. Kabacoff (Office of Naval Research, United States), M.L. Trudeau (Hydro-Québec Research Institute, Canada), and C. Moreau (National Research Council, Canada).

This conference was successful in assessing the most recent understanding concerning the science and technology of thermally sprayed nanocrystalline coatings. Special attention was paid to understanding the in-flight characteristics of particles as well as testing methods that allow critical analysis of deposit versus bulk material properties. It was also very encouraging to see the active participation of many junior researchers at this meeting, the majority of whom received traveling fellowships from our sponsors. The web site http://DOL1.eng.sunysb.edu/MTL/ quebec-uef/, shows some of the participants and social interactions.

The next workshop in this series is titled "Novel Synthesis and Processing of Nanostructured Coatings for Protection against Degradation" and is scheduled for Aug. 12–19, 2001 in Davos, Switzerland.

1. Development and Production Implementation of Nanostructured Coatings

M. Gell and E. Jordan
University of Connecticut, Storrs; CT 06269

Nanostructured coatings have the potential to replace current coatings and create new coating applications in a wide variety of high performance applications requiring improved wear, erosion, cavitation, corrosion, and thermal insulation resistance. The development status of nanostructured tungsten carbide-cobalt, alumina-titania, and yttria stabilized zirconia coatings will be described. The critical additional development and implementation steps for these nanostructured coatings will be defined in the context of successful development programs involving commercial high performance coatings. Emphasis will be placed on market drivers, including technical characteristics, material and process reproducibility, and cost.

2. Commercialization of Thermal Spray Nanomaterial Coatings: Lessons Learned, Challenges, and Future Opportunities

R. W. Rigney
R. W. Rigney and Associates, Inc., Ringgold, GA 30736

The Office of Naval Research has funded a series of programs to develop methods for making powders of ceramics, carbides, and metals with a nanosized crystal structure. The latest of these is to develop nanostructured materials to be used for thermal sprayed coatings. This program includes the identification of commercial and military applications for use of these materials. This paper will discuss the current state of development of these materials, what more needs to be done, additional materials that are desirable for the program, and where opportunities exist for use of these materials.

Where We Are Today

Nanostructured materials of tungsten carbide/cobalt in several percentages have been made with mixed results. The best

C.C. Berndt, State University of New York at Stony Brook, U.S.A. Contact e-mail: cberndt@notes.cc.sunysb.edu.

* These extended abstracts have been edited to comply with a similar form and style. Figures have been numbered consecutively. References which are related to a single contribution are placed after each abstract; *i.e.*, starting from "1" to facilitate continuity. Some authors have preferred to include a bibliography of key publications rather than specific references within the text.

materials seem to contain over 10% cobalt content with the industry standard 88/12 mixture being the focus at this point. Early test data shows a higher than expected wear index when coupled with lower hardness in many cases. This correlation is being examined to identify any other improvements in physical properties. Commercial WC/Co-18 material that has particles < 0.5 micron but > 100 nanometers has shown a high hardness and reasonable wear.

Several ceramic nanostructured materials have been made. Yttria stabilized zirconia has been made in small quantities and several varieties of 87/13 alumina-titania have been made in some quantity. These materials seem to have a correlation between nanosize content after spraying and their wear resistance. Some higher than normal tensile bond results have been seen, but need verification with additional testing.

Nanostructured metals and alloys have been made by milling fine materials. Principally aluminum and nickel based alloys have been made to date. There is also interest in making a nanopowder cored wire for electric arc spraying.

What More is Needed

Although there are interesting results seen in tests of nanostructured coatings to date, there is not an identifiable trend and results depend more on who sprays the coating and who tests it. A more rigid coating and testing plan needs to be implemented to qualify and quantify the qualities or absence of qualities seen in these coatings. The standard tests presently used for thermal sprayed coatings are useful in comparing these coatings to standard materials, but not for identifying any special characteristics that may make the use of nanostructured materials justified. New tests need to be found or devised to justify the use of these materials over conventional ones. More work on producing sprayable powder must be performed.

Additional Materials of Interest

A chrome carbide material, WC with more corrosion resistance matrixes, other ceramics, and special nickel based alloys would be of interest to commercial and military customers.

Where Opportunities Exist for These Materials

- Chrome plating replacement is a key potential application for nanoscale coatings as these are generally used for hydraulic pistons with high loads and potential flexing of long parts as an element that must be satisfied.
- Aircraft components that need thermal barrier and wear resistance ceramic coatings are a special area of application consideration.
- Shafting of all sizes with the need for more wear resistance and corrosion resistant surfaces are a large area for applications.
- Any component that needs repair but due to service conditions can not be repaired with conventional, thermal spray coatings is an area of application for more resilient and durable coatings.

A number of application areas will be reviewed for applicability of nanostructured coatings.

3. The ONR Program on Science and Technology of Thermal Barrier Coatings

S. G. Fishman
ONR Materials S&T Division

The Office of Naval Research conducts an integrated program investigating scientific aspects of thermal barrier coatings and applying results to Naval aircraft engines. Work is carried out at universities, Naval laboratories, and industrial laboratories, in a highly coordinated manner. Investigations involve process models of state-of-the-art and new processes, microstructural engineering, understanding of coating-failure processes, developing of novel *in situ* mechanical property characterization methods, and exploration of new thermal barrier coating materials. The discussion will present examples of recent scientific findings, transitions to applications, and identify areas where future work is needed.

4. Thermal Spray of Nanocrystalline Ceramics: A Program Overview

E. Jordan and M. Gell
University of Connecticut, Storrs, CT 06269

A multi-year, multi-disciplinary program has been initiated to thermal spray nanocrystalline ceramics for thermal barrier coatings and wear resistant coatings. The program involves chemical synthesis of powders and re-agglomeration, extensive thermal spray trials, materials characterization and measurement, and modeling of the fluid mechanics of thermal spray. An overview of processes used and results obtained will be presented. The high degree of interaction of different scientific disciplines will be emphasized. To date, partially nanocrystalline coatings have been produced and, for TBC's, such coatings have cyclic life properties similar to current state of the art coatings while wear resistant coatings have superior properties to current coatings. Strategies to improve on current results will be discussed.

5. Vacuum Plasma Spray Applications of Nanostructure Composite Coatings

G. E. Kim
PyroGenesis Inc., Montréal, PQ, Canada

V. Provenzano and L. Kurihara
Naval Research Laboratory (NRL), Washington, DC 20375-5343

E. J. Lavernia and M. Ice
University of California Irvine (UCI), Irvine, CA

M. L. Trudeau
Hydro-Québec Research Institute (IREQ), Varennes, PQ, Canada

Thermal spray coatings may be an attractive means of incorporating many of the proven and potential benefits associated with nanostructure materials onto the surfaces of existing components. Over the past two years, PyroGenesis Inc. has participated in several collaborative efforts with NRL, UCI, and IREQ, in the processing and evaluation of thermal sprayed nanostructure composite coatings. The composite materials which have been, and continue to be, of interest to this study are ZrO_2-Al_2O_3, Al-MMC, and WC-Co for thermal barrier, lightweight structural, and wear-resistant applications, respectively.

PyroGenesis uses atmospheric plasma spray (APS), vacuum plasma spray (VPS), and high-velocity oxyfuel (HVOF) processes to attain optimized coatings of different materials. VPS offers processing conditions which can often result in coatings with unique characteristics. Coatings of the three composite materials were VPS-applied and evaluated.

The initial spray tests demonstrated the feasibility of attaining coatings with ZrO_2-Al_2O_3 from powders processed via the slow drying of zirconia and alumina colloidal suspensions. The ceramic composite coatings were deposited onto CoNiCrAlY bond coated, stainless steel substrates. The TBC layer had a porosity level of approximately 5%. It was discovered that coatings with greater-than-or-equal-to 20 vol.% Al_2O_3 were stable (maintained their tetragonal or nanostructured form) when exposed to a temperature of 1200 °C. The potential advantages for the study of this composite material are: the stabilization of zirconia with an inert constituent like alumina; the reduction of thermal conductivity; and the enhancement of mechanical properties, such as hardness and toughness.

Cryomilled Al-MMC powders, processed at UCI, were spray tested. The powder consisted of 3003 aluminum cryomilled with 10 vol.% of 3 μm size silicon carbide. The resulting coating on mild steel substrates was very dense (< 1% porosity) with a uniform distribution of SiC within the Al matrix. The *in situ* sputter cleaning capability and reduced inert pressure ambient of the VPS process provided a coating with an absence of visible oxidation at the interface and within the coating. Microhardness measurements of the sprayed samples were quite consistent with an average value of approximately 150 HV. This is approximately twice the hardness found on typical monolithic coatings of VPS-applied aluminum. XRD results show the presence of small (~110 nm) matrix grains.

Fine-grained (~200 μm) WC-18Co powder, distributed by ONR, was deposited onto mild steel substrates using varying VPS parameters. The optical microscopic analysis revealed the presence of two distinct regions or phases (light and dark) within the coating. There was a noticeable trend towards higher light phases with increasing chamber pressure and power. Average microhardness measurements for the light and dark phases were approximately 900 HV and 1250 HV, respectively. Local EDS analysis did not reveal substantial compositional differences between the two phases.

6. Thermal Barrier Coatings Based on Zirconia Ceramics: Nanostructure, Microstructure, Properties, and Performance

Nitin Padture, Kevin Schlichting, Maurice Gell, Eric Jordan, and Paul Klemens
Institute of Materials Science, University of Connecticut, Storrs, CT 06269-3136

Plasma sprayed thermal barrier coatings (TBCs), with strategically placed nanostructured regions within the coating, are likely to be significantly more durable relative to their conventional counterparts. This is because such coatings offer: (1) higher toughness at the weakest locations in the coating, (2) lower thermal-expansion mismatch with the metal substrate, (3) enhanced creep rate to relax residual stresses, and (4) in-service microstructural stability.

The first part of this talk will concern characterization and performance of TBCs. Reconstituted nanostructured zirconia (with 7 wt.% yttria stabilizer) powders were obtained from Inframat Corporation, which were plasma sprayed on to bond-coated superalloy substrates. Results from the microstructural characterization (SEM, TEM, XRD) of these coatings will be presented. These coatings were then subjected to furnace cycling tests to simulate in-service thermal cycling conditions. The residual stresses in the thermally grown oxide at the interface between the bond coat and the zirconia coating were measured using piezospectroscopy, as a function of cycles, until spallation-failure. Piezospectroscopy is a well established technique, but has been used to measure stresses in plasma-sprayed TBCs for the first time. The information gleaned from these stress measurements and the characterization of the failed coatings was analyzed with reference to established failure models for TBCs.

The results from this analysis will be presented, along with a proposal for possible failure mechanisms in these coatings, which will be compared and contrasted with the failure mechanisms in conventional TBCs.

The second part of this talk will concern thermal conductivity and the effect of porosity on this key physical property pertaining to TBCs. The thermal conductivities of monolithic sintered zirconia, sintered zirconia containing deliberately introduced controlled porosity, and the above TBCs were measured in the temperature range 25 to 1000 °C. The thermal conductivity results were analyzed with reference to established heat-conduction theories, incorporating phonon and photon (radiation) conduction and the influence of point defects, grain boundaries, and pores on these modes of heat conduction. The ultimate goal of this study is to establish first-principles, predictive models for supporting and guiding an effort to tailor the thermal conductivities of TBCs.

7. Alumina-Zirconia Nanocomposite Thermal Barrier Coatings

V. Provenzano and L. K. Kurihara
Physical Metallurgy Branch, Naval Research Laboratory, Washington, DC 20375

J. Y. Ying and M. L. Panchula
Department of Chemical Engineering, MIT, 77 Massachusetts Ave, Cambridge, MA 02139

G. Kim
PERMA, a division of PyroGenesis, Inc., Montréal, PQ, Canada H3J 1R4

At the present time, yttria-stabilized zirconia (YSZ) is the most common material used for thermal barrier coating (TBC) applications. Typically, the hot-end components (blades and vanes) of gas turbine engines made of nickel-based superalloy are first coated with a MCrAlY metallic layer (M is Co, Ni, or Fe) and then coated with YSZ. During normal operating conditions, an alumina scale forms at the interface between the MCrAlY and the YSZ layers. The major drawback of zirconia-based TBCs is due to cracks that often form at the interface region after only a few engine cycles that eventually result in coating delamination and failure.

This paper summarizes the results of a collaborative research and development effort, where a nanocomposite approach has been successfully used to significantly reduce cracking at the bond coat-ceramic thermal barrier interface. During the last three years, this collaborative effort has involved the active participation of the Naval Research Laboratory (NRL), the Massachusetts Institute of Technology (MIT), and PERMA, a division of PyroGenesis, Inc., (Montreal, Canada). This nanocomposite approach consists in stabilizing the tetragonal phase in zirconia through microstructural control rather than the addition of chemical dopants, such as yttria or ceria. Since alumina and zirconia are immiscible phases, grain growth in zirconia is suppressed and the undesirable tetragonal-to-monoclinic phase transformation does not occur if the size of the zirconia grains are kept below a critical size (about 30 nm). Using colloidal mixing of alumina and zirconia particles and other methods, alumina-zirconia nanocomposite powders were first prepared and then deposited by vacuum plasma spray (VPS) on bond coated nickel superalloy substrates. Full phase stabilization in zirconia was achieved with only 20 % alumina addition. Also, using a laser flash technique, thermal conductivity measurements were conducted on the alumina-zirconia nanocomposite coating samples. Finally, the adherence of the nanocomposite coatings to the substrates under thermal cycling was studied.

The above results are presented and their implications for the development of a nanocomposite system with superior thermal, mechanical, and chemical characteristics for thermal barrier coating applications are discussed.

8. Properties and Microstructures of Nanostructured Partially Stabilized Zirconia Coatings

R. S. Lima, A. Kucuk, U. Senturk, and C. C. Berndt
Department of Materials Science and Engineering, State University of New York at Stony Brook, Stony Brook, NY 11794-2275

Results concerning microhardness, elastic modulus, and roughness (R_a) of plasma sprayed coatings fabricated from nanostructured partially stabilized zirconia (PSZ) feedstock are presented. Nanostructured zirconia particles were plasma sprayed (Ar/H_2) at three power levels, with two different argon flow rates at two spray distances. The results indicate that the microhardness, elastic modulus, and roughness of the nanostructured zirconia coatings exhibit a trend whereby smoother coatings exhibit higher microhardness and elastic modulus. This correlation implies that a roughness gage can be used to estimate

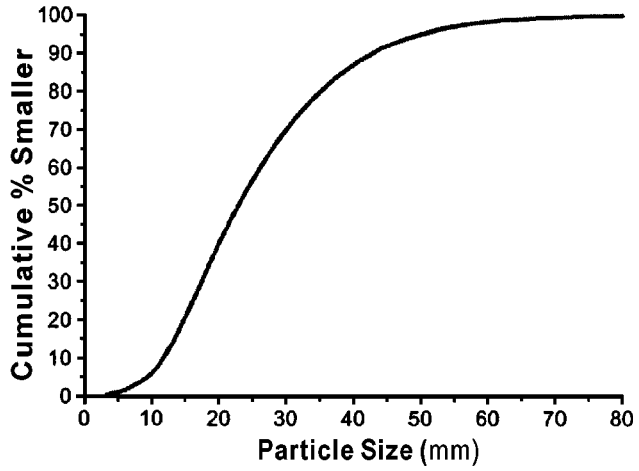

Fig. 1 Particle size distribution of the nanostructured powder

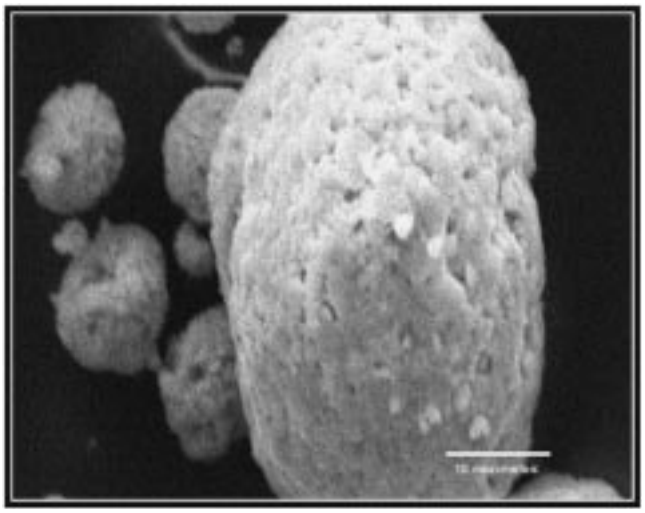

Fig. 2 SEM picture of nanostructured powder particles

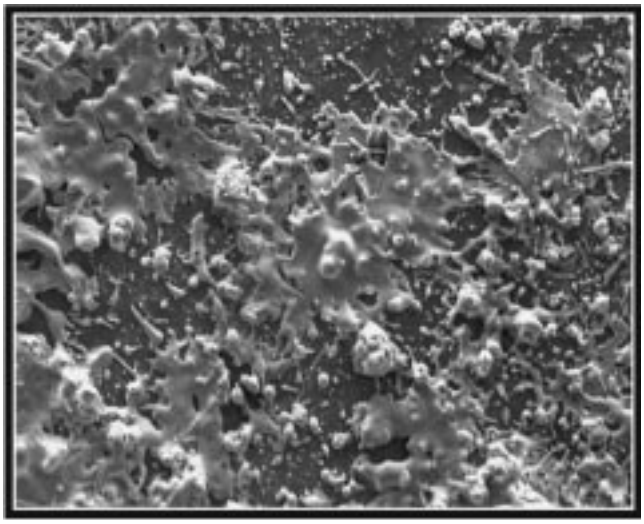

Fig. 3 Structure of the sprayed particles after impact with the substrate

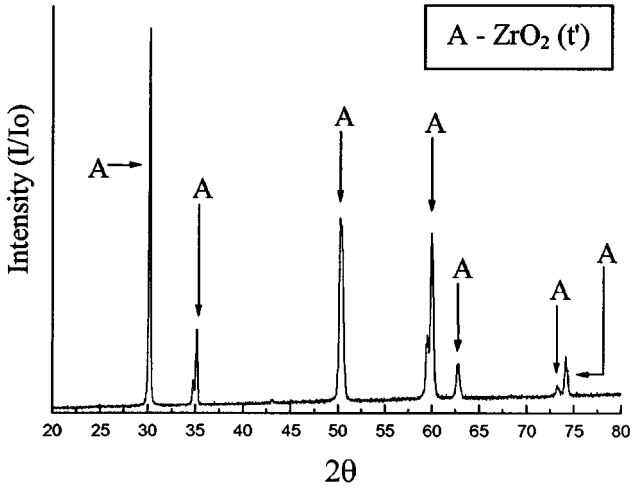

Fig. 4 XRD pattern of the nanostructured coating

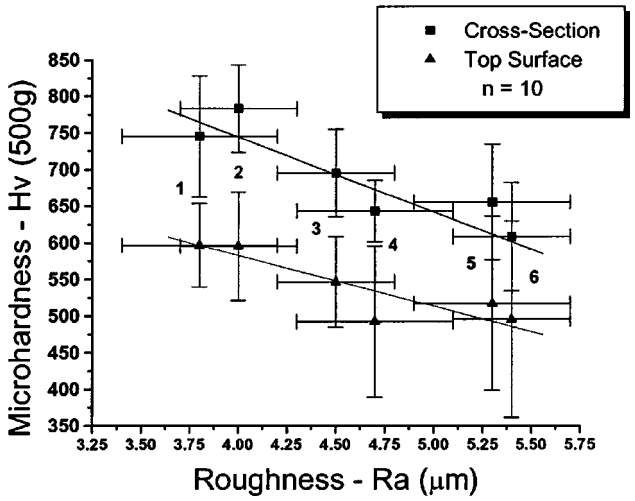

Fig. 5 Microhardness-roughness relationship in nanostructured coatings

the coating microhardness and elastic modulus; i.e., a simple nondestructive and *in situ* test is proposed for these coatings.

The powder particle distribution is similar to the commercial materials, with an average particle size close to 30 μm (Fig. 1). SEM examination shows that each powder particle is formed by the agglomeration of many tiny particles (Fig. 2). When the sprayed particles are examined, the agglomerated nanostructured particles apparently split up or explode inside the plasma flame becoming a large group of very tiny particles, having an opposite effect to the initial agglomeration (Fig. 3). This phenomenon is associated probably with the low roughness (R_a of up to 3.8 μm) presented by coatings. The nanostructured coatings exhibit only the nontransformable tetragonal t′ phase of zirconia, which is the phase with the highest thermal shock resistence of all the zirconia phases (Fig. 4). The nanostructured coatings demonstrate high values of microhardness (up to 750 HV_{500}, Fig. 5) and high values of elastic modulus (up to 95 GPa, Fig. 6) but still reveal high porosity (8 to 10%).

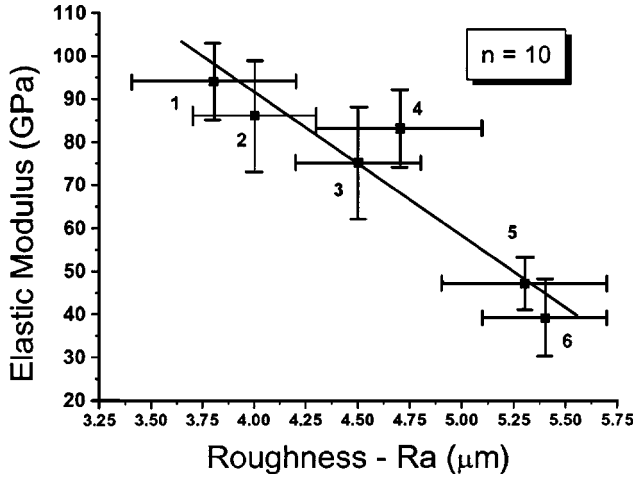

Fig. 6 Elastic modulus-roughness relationship in nanostructured coatings

Acknowledgments

R. S. Lima wishes to acknowledge the International Thermal Spray Association (ITSA) for a Scholarship Award. This work was supported by the Office of Naval Research under Grant No. N00014-97-0843 and the Center of Thermal Spray Research under NSF-MRSEC DMR 9632570.

Bibliography

1. J. Karthikeyan, C.C. Berndt, J. Tikkanen, J.-Y. Wang, A.H. King, and H. Herman: *Nanostr. Mater.*, 1997, vol. 8 (1), pp. 61–74.
2. J. Karthikeyan, C.C. Berndt, T. Tikkanen, J.Y. Wang, A.H. King, and H. Herman: *Nanostr. Mater.*, 1997, vol. 9, pp. 137–40.
3. J. Tikkanen, K.A. Gross, J. Karthikeyan, V. Pitkanen, J. Keskinen, S. Raghu, M. Rajala, and C.C. Berndt: *Surface Coatings Technol.*, 1997, vol. 90, pp. 210–16.
4. J. Karthikeyan, C.C. Berndt, J. Tikkanen, S. Reddy, and H. Herman: *Mater. Sci. Eng. A*, 1997, vol. 238 (2), pp. 275–86.
5. J. Karthikeyan, C.C. Berndt, S. Reddy, J.-Y. Wang, A.H. King, and H. Herman: *J. Am. Ceram. Soc.*, 1998, vol. 81 (1), pp. 121–28.
6. T. Chraska, A.H. King, and C.C. Berndt: *Mater. Sci. Eng. A*, 2000, vol. A286, pp. 169–78.

9. Thermal Stability of Nanostructured Cr_3C_2-NiCr Coatings

Jianhong He, M. Ice, and E. J. Lavernia
Department of Chemical and Biochemical Engineering and Materials Science University of California, Irvine, CA 92697-2575

Thermal stability of thermally sprayed nanostructured Cr_3C_2/NiCr coatings was investigated. The results show that microhardness of the conventional coating increased only slightly with an increase in the exposure temperature, whereas that of the nanostructured coating increased from 1020 to 1240 DPH_{300}. Heat treatment led to an increase in scratch-resistance and decrease in coefficient of friction of the nanostructured coatings. The observed increases in microhardness and scratch-resistance and decrease in coefficient of friction of the nanostructured coatings are attributed to a high density of oxide nanoparticles (8.3 nm) that precipitate within the coating as the exposure temperature increases.

10. Supersonic Induction Plasma Spraying of High Density Nanostructured Ceramics

M. Boulos and F. Gitzhofer
Plasma Technology Research Technology (CRTP), Department of Chemical Engineering, Faculty of Engineering, Université de Sherbrooke Sherbrooke, PQ, Canada J1K 2R1

Supersonic induction plasma spraying has emerged over the past few years as a new and potentially interesting technology for the deposition of high density ceramic coatings. Yttria stabilized zirconia coatings formed using this technique with air as the plasma gas exhibited apparent densities close to 99% of the theoretical density of the material. The relatively fine particle size of the material used and the high impact velocity on the substrate contributed to the formation of fine grained deposits. Further experimentation with this technique aims at exploring avenues for its use for the reactive deposition of nanostructured materials. A review will be presented of the current state of the art in this area and future developments under study.

11. Synthesis and Processing of Nanostructured Nitride Ceramics

J. Y. Ying, M. L. Panchula, and D. T. Castro
Department of Chemical Engineering, MIT, Cambridge, MA 02139

With their high strength and resistance to heat, wear, and corrosion, the nitride family of ceramics demonstrates great promise in a number of engineering applications. However, there are many difficulties in sintering and forming pure nitrides due to their covalent bonding and high melting points as well as the low quality of the commercially available powders. We have designed and constructed a novel forced flow reactor for the large-scale synthesis of nanocrystalline materials. The reactor operates using a replenishable thermal evaporation source in a forced gas flow. The gas stream can quickly remove particles generated from the hot growth zone over the crucible to preserve the ultrafine particle size with minimal agglomeration. A downstream microwave-generated nitrogen plasma allows *in situ* nitridation of evaporated metals. A variety of nanocrystalline metals (Si and Al) and nitrides (silicon nitride, titanium nitride, and aluminum nitride) have been produced with particle size of ~10 nm. The high-quality nitride nanoparticles produced in our reactor greatly enhanced sintering of these advanced ceramics for potential applications as structural and electronic packaging materials.

12. Microstructural Evolution of Nanocrystalline Cu-Al Particles during HVOF Thermal Spraying

M. L. Lau and E. J. Lavernia
Department of Chemical and Biochemical Engineering and Materials Science University of California Irvine, Irvine, CA 92697-2575

R. Schweinfest
Max Planck Institut für Metallforschung, D-70174, Stuttgart, Germany

The present paper describes the microstructural evolution of nanocrystalline Cu- 10 wt.% Al coatings produced by high velocity oxygen fuel spraying. Elemental Cu with a particle size of 45 ± 11 μm was blended with 10 wt.% Al powder and subsequently mechanically alloyed to produce powders with nanocrystalline and amorphous grain structures. The mechanically alloyed powders were thermally sprayed onto stainless steel substrates. Transmission electron microscopy performed on the cross sections of the nanocrystalline coating indicates a complex microstructure composed of nanocrystalline Cu and amorphous Al_2O_3. A mathematical model is developed to explain the formation of the nanocrystalline coating and possible oxidation mechanisms will be discussed. The results from the mathematical modeling will be used to compare with the temperature profile obtained from diagnostic measurements.

13. High Energy Plasma Spray Coating Using Micrometer- and Nanometer- Scale Tungsten Carbide-Cobalt Powder

D. G. Atteridge, R. Davis, M. Scholl, and G. Tewksbury
Oregon Graduate Institute of Science and Technology, Portland, OR

M. Becker
Portland State University, Portland, OR, and Knolls Atomic Power Laboratory, Schenectady, NY

Nanometer-scale tungsten carbide (WC) particles have been successfully used in cemented carbide applications and have garnered interest for thermal spray applications. In this Office of Naval Research sponsored study, the high-energy-plasma-spray (HEPS) process was employed to form coatings using powders containing nanometer scale WC particles. The nanometer-scale WC particles were embedded in a cobalt matrix and produced as micron-scale, nominally spherical particles.

High energy plasma spraying was examined due to its ability to spray many forms of feedstock, both in type and scale, while producing high quality coatings. Heat transfer analysis indicated that one can expect complete particle melting and, thus, highly fluid particle splats on impact with the substrate/coating surface, given the energy density in the high velocity plasma jet. The combination of particle heating and acceleration was expected to yield low porosity, high adhesion strength coatings. The HEPS was carried out at the Oregon Graduate Institute using a 200 kW Plazjet plasma spraying system. This system operates from 200 to 500 V and 100 to 500 amperes, with gas flows from 100 slpm to over 500 slpm. Nitrogen/hydrogen mixtures can also

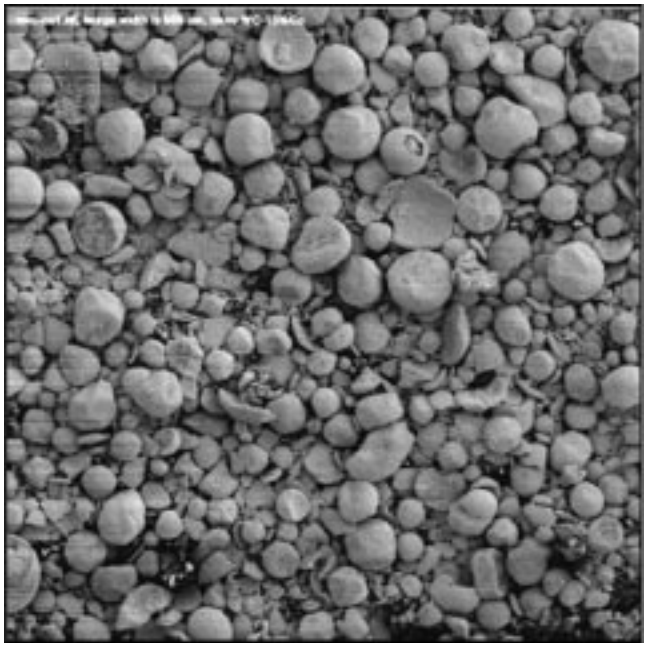

(a)

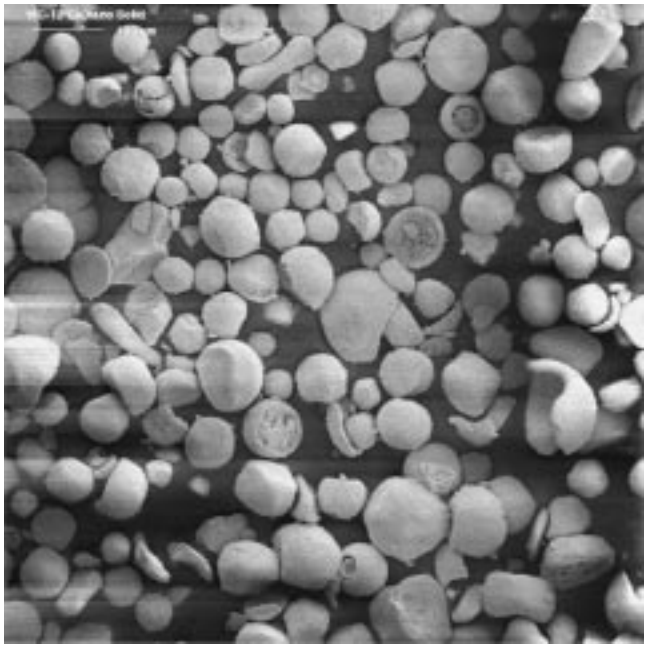

(b)

Fig. 7 SEM photomicrograph of hollow and solid agglomerated nanometer-scale WC-Co powder

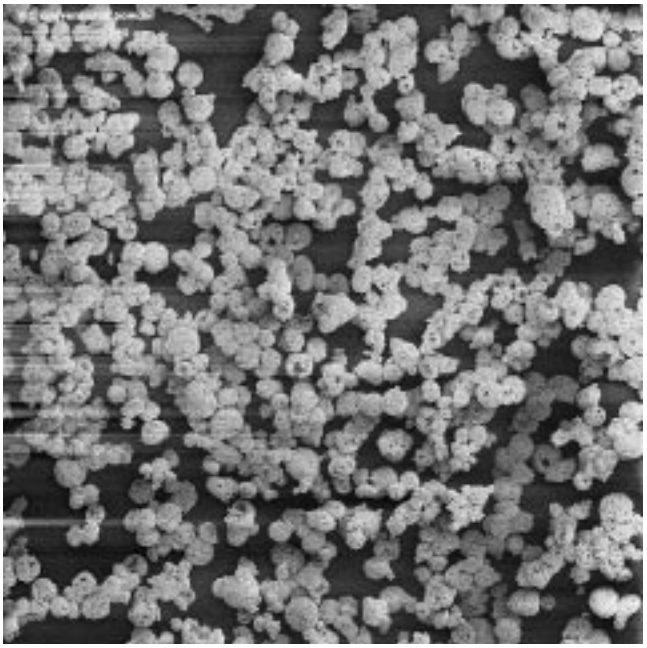

Fig. 8 SEM photomicrograph of conventional solid micrometer-scale WC-Co powder

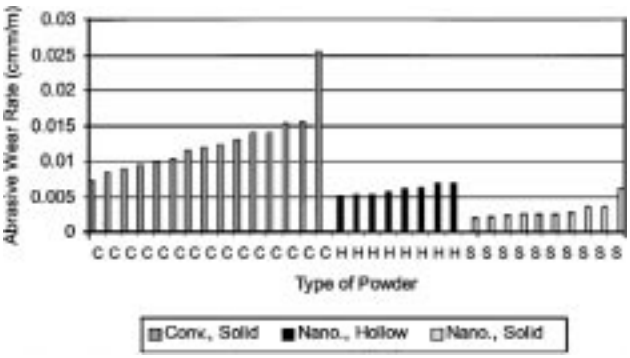

Fig. 9 Effect of WC particle size (micrometer vs nanometer) and powder type on resultant WC-12Co coating abrasive wear rates. C—conventional solid, H—hollow nanoscale, and S—solid nanoscal

be used at ratios less than 1:1. The system is capable of spraying both wire feedstock from 0.035 to 0.125 in. in diameter or powder feedstock from 10 μm to over 150 μm in diameter; or both may be used simultaneously.

High energy plasma spray coatings were manufactured using micrometer-scale and nanometer-scale WC-Co agglomerated powder as feedstock. The powders were sprayed in the as-received condition without further processing. Several different batch-runs of nanometer- and micron-scale WC-Co powder were sprayed as a function of stand-off distance, gas composition, and flow rate. The nanometer-scale WC-Co powder composition varied from 5 to 15 wt.% Co with the balance being nanometer scale WC particles. Commercially available micrometer-scale WC-Co powder containing either 12% or 17% Co composition was also sprayed.

Coatings were deposited on carbon steel substrates which were grit-blasted immediately prior to coating. Several spray parameter sets were run for each material, although the small quantity of the nanometer powders limited testing. Subsequent analysis and testing included optical microscopy, scanning electron microscopy, transmission electron microscopy, and a modified ASTM G65-94 dry-sand, rubber-wheel wear testing.

The results reported here deal with three 12 wt.% Co powders; one conventional-sized and two nanometer-scale WC containing powders. The conventional and one of the nanometer WC powders were composed of solid spheres while the other powder was composed of hollow spheres. SEM photomicrographs of the three powder types are shown in Figs. 7 and 8. All powders fed easily and resulted in high quality coatings. A series of spray parameter variations were used to produce a variety of coatings with the different powders. An assessment of the coating wear results from dry-sand, rubber-wheel testing revealed that the nanometer-scale WC coatings were superior in wear resistance compared to conventional-WC coatings, and that the solid powder coatings were superior to the hollow powder coatings. This is demonstrated in Fig. 9, where the individual test data are plotted as data sorted by increasing wear rate and as a function of powder type.

The spray parameters studied included primary nitrogen gas flow rate, secondary hydrogen gas flow rate, specimen stand-off distance, powder feeder parameter settings, and number of spray passes. The solid-sphere nanometer-scale WC spray parameter results indicate that the major variable controlling coating quality was nitrogen gas flow velocity, as shown in Fig. 10. Decreasing nitrogen gas flow rate from 185 to 120 slpm was found to form coatings with a substantially increased wear resistance. Variation of specimen stand-off distance from 200 to 300 mm had little or no effect, as did the powder feeder flow rate from 140 to 200 g/m. Doubling of the number of spray passes from 50 to 100 was found to degrade wear resistance. The addition of hydrogen was found to increase wear resistance. Decreasing nitrogen gas flow rate dramatically decreased coating porosity. The 180 slpm coating exhibited an average of 13% porosity with a standard deviation of 9% while the 130 slpm coating exhibited an average of 12% porosity with a standard deviation of 2%. The addition of hydrogen gas decreased coating porosity an average of 4.5% with a standard deviation of 1.6%. It is anticipated that further parameter optimization will decrease the porosity further, since porosity levels that were undetectable by optical microscopy techniques were achieved with the nanometer-scale, WC hollow sphere powder coatings.

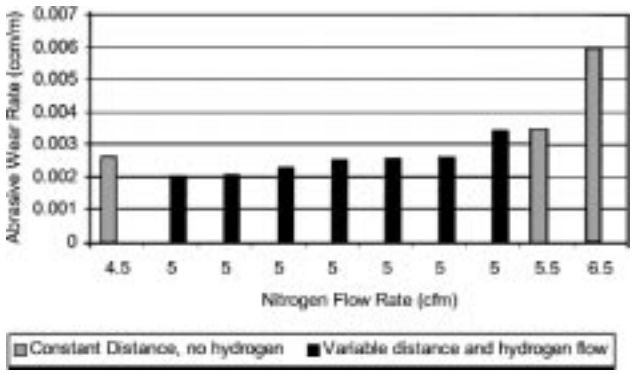

Fig. 10 Effect of HEPS parameters on dry-sand-rubber-wheel wear rates for nanosized WC(12% Co) coatings produced using solid sphere agglomerated powder feedstock

14. Thermal Spray Processing of Nanostructured Alumina Coatings

R. Hickman and T. McKechnie
Plasma Processes, Inc., Huntsville, AL

Innovative plasma deposition technologies were developed to produce alumina coatings using nanosize powders and liquid suspensions. The coatings were 5 to 10 microns thick and well bonded to Inconel 625 substrates. Adhesion tests performed on the coatings indicate bond strengths above 10 ksi, the limit of the epoxy adhesive used for attaching test stubs to the coating. Cyclic oxidation behavior was evaluated by furnace heating the samples to 1000 °C and quenching to ambient temperatures 25 times. The coatings showed substantial resistance to spalling and remained well bonded to the substrate. SEM examination revealed a coherent fine microstructure and showed evidence of particle melting and fusing to form individual splats and layers. X-ray diffraction scans indicate that the as-sprayed deposits consist of high-temperature, stable alpha alumina (Al_2O_3) as the dominant phase. Plasma deposition of an alumina sol resulted in complete conversion from boehmite (AlOOH) into the stable alpha phase. The results indicate that different processing variables such as starting feed material and liquid atomization affect the crystallinity and nanograin size. Thus, it is possible to ma-

Table 1 Adhesion test results

Specimen	Adhesion (ksi)	Comments
Al_2O_3/IPA	3.3	Coating failure
Nanosize powder	11.7	Epoxy failure, coating intact
Alumina sol	7.8	Coating failure
Al_2O_3/H_2O	11.6	Epoxy failure, coating intact

Fig. 11 Liquid plasma sprayed alumina (<10 μm thick)

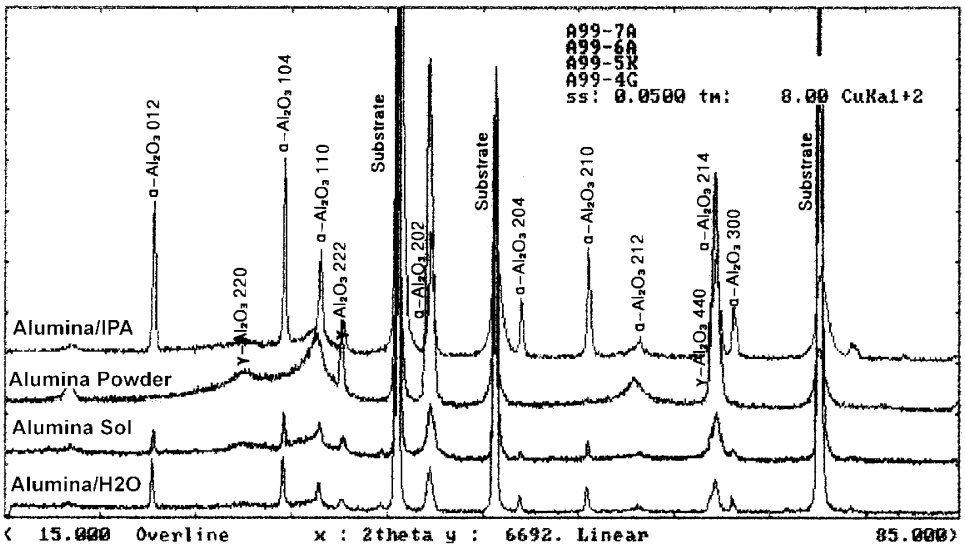

Fig. 12 XRD scans of the as-sprayed alumina coatings

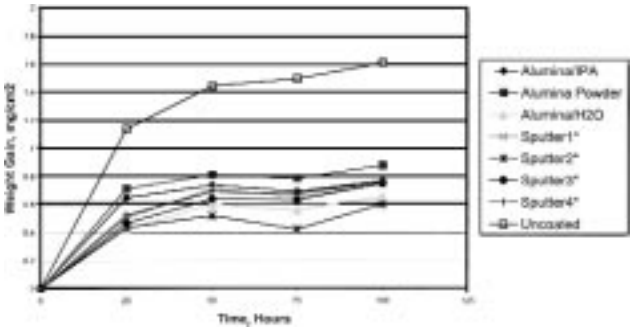

Fig. 13 Oxidation behavior of the alumina coatings. *Reactive sputter deposited alumina coatings were tested for comparison

nipulate the microstructure to form coatings with superior high temperature oxidation and corrosion resistance. (Table 1 and Figs. 11 to 13.)

Bibliography

1. S.L. Chawla and R.K. Gupta: *Material Selection for Corrosion Control*, ASM International, Materials Park, OH, 1993.
2. J. Karthikeyan, C.C. Berndt, S. Reddy, J. Wang, A.H. King, and H. Herman: *J. Am. Ceram. Soc.*, 1998, vol. 81 (1), pp. 121-28.
3. J. Karthikeyan, C.C. Berndt, J. Tikkanen, J.Y. Wang, A.H. King, and H. Herman: *Nanostr. Mater.*, 1997, vol. 8 (1), pp. 61-74.
4. M. Gell: *Mater. Sci. Eng.*, 1995, vol. A204, pp. 246-51.

15. Nicalon Reinforced Strontium Aluminosilicate (SAS) Ceramic Matrix Composites *via* Infiltration of a SAS Precursor/SAS Nanoparticle Suspension

T. Hinklin and R. M. Laine
Department of Materials Science and Engineering, University of Michigan, Ann Arbor, MI 48108

A simple and inexpensive one-step route to preceramic polymers has been developed [Oxide One Pot Synthesis (OOPS) Process]. In the OOPS process, SiO_2, $Al(OH)_3$, and MO (M = Mg, Sr, Ba) are reacted with triethanolamine in ethylene glycol solvent at 200 °C. In addition to being an alternative to traditional melt processing of ceramics and glasses, these precursors have also been used to form nanoparticles using a flame spray pyrolysis technique. This presentation demonstrates the effectiveness of using a suspension of $SrAl_2Si_2O_8$ (SAS) nanoparticles (20 to 150 nm) in a SAS precursor/methanol solution to create Nicalon reinforced SAS ceramic matrix composites. The phase transformations and microstructures formed after pyrolysis at selected temperatures and times are examined using TGA, DTA, XRD, SEM, TEM, and DRIFTS.

16. Nanostructured Coatings of SiC Synthesized by Induction Thermal Plasma Chemical Vapor Deposition

E. Bouyer, M. Müller, G. Schiller, and R. Henne
German Aerospace Center, Institute for Technical Thermodynamics, Vaihingen, Pfaffenwaldring 38–40, 70569 Stuttgart, Germany

Introduction

There is an increasing demand of nanostructured materials, especially in the field of structural ceramics. The specific properties of such materials justify their success.[1] Various techniques have been developed for nanomaterial preparation and one among them, called Plasma Spray Synthesis, reports promising results for oxide ceramic nanomaterial synthesis from a liquid precursor.[2] Nevertheless, postspray treatments are needed to produce dense oxide deposits with nanosized grains.[3]

This paper presents a novel one step synthesis route for nanostructured ceramic coatings from the high temperature decomposition of a liquid precursor. This process uses an inductive thermal plasma as a heating source. The chloro-carbo-silane mixture precursors are a low cost by-product of the silicon industry (*via* the Müller-Rochow synthesis). This process, called Thermal Plasma Chemical Vapor Deposition (TPCVD),[4] when it is applied on an inductive plasma, takes advantage of both the high plasma volume and the versatility concerning the plasma gas as well the precursor nature potentially used due to the absence of electrodes. Thus, induction plasma technology is well suited to achieve clean chemistry under plasma conditions. A prominent feature of TPCVD is the deposition rate (or growth rate) which is two to three orders of magnitude greater than the case of conventional CVD.[5]

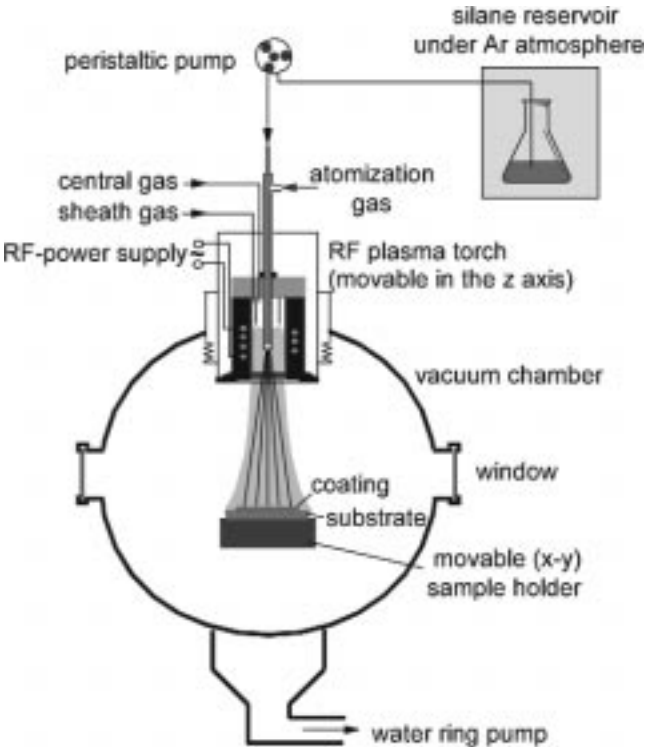

Fig. 14 Radio frequency induction plasma installation

Experimental Setup

The plasma installation used for the synthesis of ceramic coatings is shown in Fig. 14. The process description can be found elsewhere.[6] Substrates are Mo (or stainless steel) plate ($40 \times 40 \times 3$ mm), which are lightly sand-blasted and then cleaned with isopropanol prior to the experiment. The precursor employed in this study is a mixture of chloro-carbo-disilanes.

Results and Discussion

From this study, a key parameter in this process is the residence time of the reactive species (silane precursor) in the plasma. This dwell time depends strongly on both the spray distance and on the plasma jet velocity.

However, the substrate temperature is also of great importance in relation to the coating microstructure. Previous work has shown that the substrate temperature should be between 1100 and 1300 °C.[6] Therefore, because the substrate is directly heated due to conduction from the plasma gas, the spray distance plays an important role regarding the substrate temperature

Figure 15 shows one of the three typical structures of a SiC coating that can be obtained by the TPCVD method. This cauliflower-like structure is the result of film growth exclusively in the vertical direction of the substrate. In this case, the reactant-decomposition and the reaction on the substrate surface which is exposed to the plasma flame occur simultaneously. The deposition rate of SiC is in a range between 1 to 5 μm/min and the coating thickness is lower than 20 μm thick.

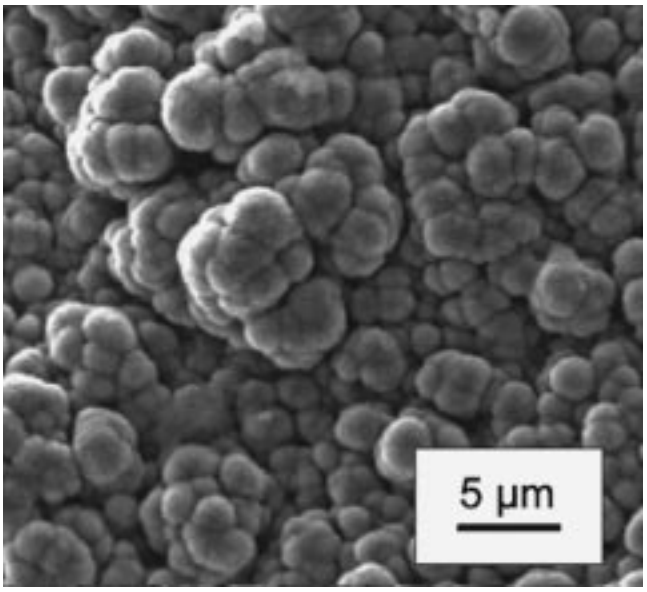

Fig. 15 SEM picture of a as-synthesized SiC coating (top view)

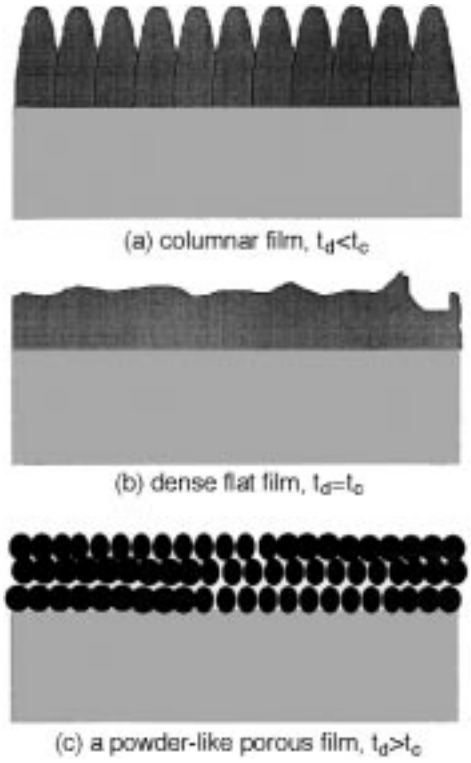

Fig. 16 Schematic representation of typical TPCVD microstructure, with t_d, dwell time, and t, critical time

As shown in Fig. 16, three main types of microstructure can be found from the TPCVD process and these depend on the dwell time of the precursor in the plasma. When the dwell time in the plasma is lower than a critical time (t_c), the reaction completion cannot occur before the species strike the substrate. This leads to a columnar structure, (Fig. 15). On the other hand, when the dwell time is too high, the coarse particles are formed in the plasma and strike the substrate without any further densification possible. For a critical dwell time, t_c, the particles ("hot clusters") are homogeneously synthesized in the plasma after which they are deposited on the substrate to become flat and dense.

The main phase found by x-ray diffraction in the as-deposited coating is β-SiC with some traces of α-SiC. In some cases, the presence of elemental silicon in the as-sprayed material, as shown in Fig. 17, supports a reaction route which suggests first the formation of atomic silicon from the decomposition of silane prior to the reaction with CH_x groups giving SiC clusters. A similar hypothesis was reached by Rao *et al.*[7] Compounds such as molybdenum silicide (Mo_5Si_3) and molybdenum carbide (Mo_2C) can be formed at the interface between the Mo substrate and the SiC coating. One can also notice the presence of ultrafine SiC powder on the reactor wall. The non-negligible thermal gradient between the plasma and the water cooled reactor wall involves an important mechanism of thermophoresis which is responsible for the fine particle deposition on the cold reactor wall.[8] The velocity, thermal, and concentration boundary layers existing between the plasma and the substrate play an important role in

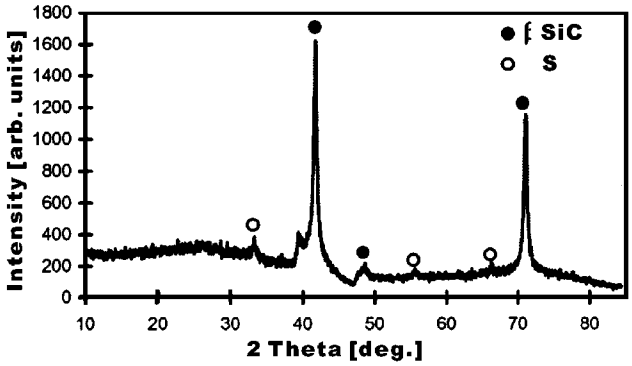

Fig. 17 XRD pattern of SiC produced from chlorocarbodisilane mixture (P = 22 kW, p = 20 kPa, d = 170 mm, stainless steel substrate)

terms of supersaturation as well as on the nucleation process and, therefore, on the resulting coating microstructure. With a thin boundary layer thickness (BLT), the heterogeneous nucleation on the substrate prevails (with possibilities of epitaxy). On the other hand, a thick BLT will privilege the homogeneous nucleation under plasma conditions. Consequently, a control or better online measurement of this BLT would be of great interest for process control.

Conclusions

According to the presented results, nanostructured β-SiC coating can be synthesized from a low-cost liquid silane type precursor using the TPCVD process. The SiC deposition rate associated with this technique attains more than a few μm/min. The coating microstructure can be controlled by the plasma parameters. The major issue of this process is to control the microstructure of the coating as a function of the precursor composition. This work supports the mechanism that silicon nucleation is the first step in silicon carbide particle formation. The continuation of this project is to synthesize Si-C-N or SiC/Si_3N_4 mixtures in a reactive plasma gas.

References

1. H. Gleiter: *Nanostr. Mater.*, 1992, vol. 1, pp. 1-19.
2. J. Karthikeyan, C.C. Berndt, J. Tikkanen, S. Reddy, and H. Herman: *MSE-A*, 1997, vol. 238, pp. 275-86.
3. J. Karthikeyan, C.C. Berndt, S. Reddy, J.-Y. Wang, A.H. King, and H. Herman: *J. Am. Ceram. Soc.*, 1998, vol. 81, pp. 121-8.
4. P. Fauchais, A. Vardelle, and A. Denoirjean: *Surface Coatings Technol.*, 1997, vol. 97, pp. 66-78.
5. T. Yoshida: *Pure Appl. Chem.*, 1994, vol. 6, pp. 1223-30.
6. E. Bouyer, M. Müller., G. Schiller, and R. Henne: "Conversion of silanes into SiC by RF Plasma Technology," p. 853 of *Proc. UTSC'99*, Düsseldorf, 1999.
7. N. Rao, S. Girshick, J. Heberlein, P. Mc Murry, S. Jones, D. Hansen, and B. Micheel: *Plasma Chem. Plasma Processing*, 1995, vol. 15 (4), pp. 581-606.
8. J.-F. Bilodeau and P. Proulx: *Aerosol Sci. Technol.*, 1996, vol. 24, pp. 175-89.

17. Hyperkinetic Deposition of Nanopowders by Supersonic Rectangular Jet Impingement

V. Shukla, G. Elliott, and B. Kear
Center for Nanomaterials Research, Rutgers University, Piscataway, NJ 08854-8065
Contact e-mail: bkear@rci.rutgers.edu

With a view towards improving the next generation of coatings, a new coating technique, *hyperkinetic deposition*, is being developed. In this method, the material to be coated is supplied in nanopowder form and is injected into a supersonic rectangular jet (design Mach number of 3.2, with a rectangular exit of 3.17×16.76 mm) which impinges on the surface to be coated. A powder feeder, designed for use with nanopowders, is used to inject powders near the nozzle throat. The powder gains speed through momentum transfer from the jet and bonds on the substrate (surface to be coated) due to the kinetic energy of the nanopowder. Several coatings using 3 to 5 micron size copper and nanopowder WC on steel and aluminum substrates have been produced. The benefit of this process is that the material does not undergo any chemical changes during formation of coatings.

The particle velocities have been estimated using particle image velocimetry. The flapping modes produced by supersonic jet impingement are being studied to improve the coatings produced. The effect of nozzle stand-off distance on material porosity will be presented.

18. On the Use of Chemical Feeds in Thermal Spraying of Nanostructured Ceramic Coatings

B. H. Kear
Center for Nanomaterials Research, Rutgers University, Piscataway, NJ 08854-8065
Contact e-mail: bkear@rci.rutgers.edu

Coating formation by CVD in a hot-wall tubular reactor is a familiar process. Two competing growth mechanisms have been identified: (1) heterogeneous nucleation and growth of a coating on the reactor wall upstream near the gas inlet, and (2) homogeneous nucleation and growth of particles in the gas phase downstream near the gas outlet. An important finding has been that at a specific temperature and precursor concentration there is a master curve relating coating deposition rate to residence time. For residence times up to a maximum in the curve, there is essentially powder-free coating deposition. The permissible residence time regime for coating formation decreases markedly with increasing temperature.

Recently, these principles have been incorporated in several related thermal spray-type processes for making ceramic coatings, utilizing gaseous or liquid precursor feeds, rather than conventional powder feeds. In all cases, the precursor decomposition zone is in the form of a stream or jet of hot reacting gases that emanate from a combustion-flame, radiantly-heated, or plasma-arc reactor. A coating is formed by interactions between the initial decomposition products of the precursor compound, so-called reactive intermediates, and a heated substrate surface, which is heated directly by the impinging hot gas stream. Critical processing parameters are gas temperature and residence time, precursor concentration, substrate temperature, and stand-off distance between reactor outlet and substrate surface. This paper will describe the progress made in the development of these processes for the fabrication of nanostructured oxide and non oxide ceramic coatings. The natural extension of the new technology into preform fabrication will also be briefly discussed.

19. Continuous Wave Lasing from Rare Earth Doped Oxide Single Crystal Nanoparticles

G. Williams
Division of Applied Physics, University of Michigan, Ann Arbor MI 48109

S. C. Rand
Division of Applied Physics, Department of Physics, and Department of Electrical Engineering and Computer Science, University of Michigan, Ann Arbor MI 48109

T. Hinklin
Department of Materials Science & Engineering, University of Michigan, Ann Arbor MI 48109

R. M. Laine
Department of Materials Science & Engineering and Department of Chemistry University of Michigan, Ann Arbor, MI 48109

We recently described methods of producing nanosized oxide powders by flame spray pyrolysis of novel alkoxide aluminate and silicate complexes as well as other soluble metal complexes. This scaleable synthesis route provides reproducible, high purity nanosized powders. We can currently make single crystal aluminosilicate powders (2 to 80 nm diameter and surface areas of

40 to 60 m^2/g) at production rates ≥ 100 g/h. The powders are characterized using a variety of techniques. The presentation will focus on the utility of the FSP method to provide exact control of dopant concentrations, the formation of selected matrices, and the potential to optimize luminescence, lasing, and other desired properties.

20. Nanostructure in Plasma Sprayed Hydroxyapatite Coating

L.M. Sun and C.C. Berndt
Department of Materials Science, State University of New York at Stony Brook Stony Brook, NY 11794-2275

K.A. Khor
School of Mechanical and Production Engineering and Nanyang Technological University, Singapore 639798

Hydroxyapatite (HA, $CA_{10}(PO_4)_6(OH)_2$) has been used for bone substitution and as an implant material (together with metal) due to its compositional similarity with the inorganic phase in natural bone. It is known that HA in natural bone is not-well-crystallized carbonated apatite and the crystal is in the morphology of a nanosized platelet (~45 × 20 × 3nm).[1] Therefore, to obtain high bioactivity and bone bonding, it is reasonable to make both the composition and the microstructure (especially the surface topography) of the HA implant similar to those of the natural bone.[2] It is expected that HA with grain size of nanometer scale is more desirable for the implant application.

Plasma spraying has been proven to be an effective way to produce a coating with a very fine grain size—typically several hundreds of angstroms if the particles are wholly melted and recrystallized due to the high cooling rate.[3,4] However, due to the complex structure of HA as well as the high cooling rate and the loss of OH− during the spraying process, some metastable or amorphous phases also form in the HA coatings,[5] which are more soluble than the crystalline HA phase.[6,7]

Currently, the bone bonding at the interface between the HA coating and the body tissue is established through the process of dissolution, precipitation, and ion exchanges between the surface of the coating and the body fluid.[8] Partial dissolution of the coating surface (usually the amorphous phase) was needed to provide a supersaturated calcium and phosphorus environment for the consequent precipitation process. A nanosized carbonated apatite layer is found to form on the surface of the coating and this exhibits a very similar structure to the inorganic phase of the bone.[9] Therefore, this layer can enhance fast osteoblast adhesion to the coating at the interface and help the bone remodeling. However, further dissolution of the amorphous phase will also cause the degradation of the coating and finally destroy the implant-bone bonding.

It is hypothesized that a coating composed mostly of nanosized crystalline HA with also some nanosized amorphous phases distributed over the crystalline phase will provide enhanced bioactivity and osteoblast bonding. The nanocrystals of HA will be more dissolvable due to a very high interface area and will be the early nucleation sites for the precipitated carbonated apatite.[10] The dissolution of the nanosized amorphous phase will help in the precipitation of apatite, but it will not cause the degradation of the whole coating due to its very small size. Instead, the dissolved amorphous region will become nanoporosity, which will even make it easier for the bone to grow into the coatings.

To effectively control the composition and the structure of HA coatings, both the starting powders and the process parameters, maybe the post-treatment as well, need to be strictly controlled. It is important for all particles to be completely melted and most of them recrystallized to nanosized crystals while some nanosized region remained as amorphous phase. The cooling rate should be optimized to avoid both the formation of large regions of amorphous phase and the decomposition of the HA. The OH− state of the HA should also be considered since the loss of OH− will affect the formation of amorphous phase.

Acknowledgments

This work is supported under NSF-MRSEC DMR Grant No. 9632570.

References

1. S. Mann: *Nature*, 1988, vol. 332 (10), pp. 119-24.
2. T.J. Webster, R.W. Siegel, and R. Bizios: *Biomaterials*, 1999, vol. 20, pp. 1221-27.
3. B. Koch, J.G.C. Wolke, and K. de Groot: *J. Biomed. Mater. Res.*, 1990, vol. 24, pp. 655-67.
4. H. Ji, C.B. Ponton, and P.M. Marquis: *J. Biomed. Mater. Res.*, 1992, vol. 3, pp. 283-87.
5. C.C. Berndt, G.N. Haddad, A.J.D. Farmer, and K.A. Gross: *Mater. Forum*, 1990, vol. 14, pp. 161-73.
6. R Z. LeGeros: *Clin. Mater.*, 1993, vol. 14, pp. 65-68.
7. K A. Gross, C.C. Berndt, D.D. Goldschlag, and V.J. Iacono: *Int. J. Oral Maxillofacial Implants*, 1997, vol. 12, pp. 589-97.
8. P. Ducheyne, S. Radin, and L. King: *J. Biomed. Mater. Res.*, 1993, vol. 27, pp. 25-34.
9. J. Weng, Q. Liu, J.G.C. Wolke, X. Zhang, and K. de Groot: *Biomaterials*, 1997, vol. 18, 1027-35.
10. W. Tong, Z. Yang, X. Zhang, A., Yang, J. Feng, Y. Cao, and I. Chen:. *J. Biomedical Mater. Res.*, 1998, vol. 40 (3), pp. 407-13.

21. In-Flight Particle Diagnostics: A Promising Tool for Nanoprocessing

C. Moreau, L. Leblanc, and M. Lamontagne
National Research Council of Canada, Boucherville, PQ, Canada J4B 6Y4,
Contact e-mail: christian.moreau@nrc.ca

L. Pouliot, J. Blain, and F. Nadeau
TECNAR Automation Ltee, St-Hubert, PQ, Canada, J3Y 8Y5
Contact e-mail: lpouliot@tecnar-automation.com

Introduction

There has been a growing interest for engineered coatings, in particular for the manufacturing and deposition of nanoscaled powders and coatings.[1,2] Outstanding properties can be obtained if the nanocrystalline structure of the starting material is preserved during spraying and reproduced into the coating. Thermal spraying is a technique well suited for such a deposition as the processing time at high temperature of the sprayed powders is only several milliseconds, thus limiting the grain growth. The coating attributes strongly depend on the actual particle temperature and velocity during spraying.[3]

Thermal spraying is comprised of a variety of different techniques (air plasma spraying, HVOF, cold spray, *etc.*) in which the temperature and velocity of the sprayed particles vary tremendously. The temperature of the particles can reach 3,500 °C for refractory materials in plasma spraying while it reaches only a few hundred degrees during cold spraying. On the other hand, the velocity can range from a few tens of meters a second up to 1000 m/s. In cold spray processes, particles are not melted since their temperature lies somewhere between room temperature and a few hundred degrees Celsius. Consequently, the coating adhesion, cohesion, and properties strongly depend on the kinetic energy of the particles. Monitoring of particle size and velocity is, thus, of great interest.

In this paper, we present different examples on how particle diagnosis techniques can be used to optimize and control coating attributes during spraying. We report also on the development of a new instrument (CPS-2000) which, used in conjunction with the DPV-2000 in-flight particle sensor from Tecnar Automation Ltee,[4] enables the measurement of particle size, velocity, and flux regardless of the particle temperature. Such an instrument can be used during cold spraying.

Experimental Setup

Measurement of temperature, velocity, size, and flux of sprayed particles is carried out using the DPV-2000 sensor.[5] This system analyzes the thermal radiation emitted by the hot particles as they travel in the field of view of the sensor head. For monitoring cold particles, a laser beam is used to illuminate the in-flight particles in the field of view of the DPV-2000. The radiation emitted by a high-power solid-state laser diode (3 to 5 Watts CW) at around 800 nm is coupled into a 400 micron core, 0.37 NA optical fiber. The other termination of the optical fiber is SMA-coupled into a carefully designed beam shaper in order to generate uniform lighting over an area of 1.5×1.5 mm. The

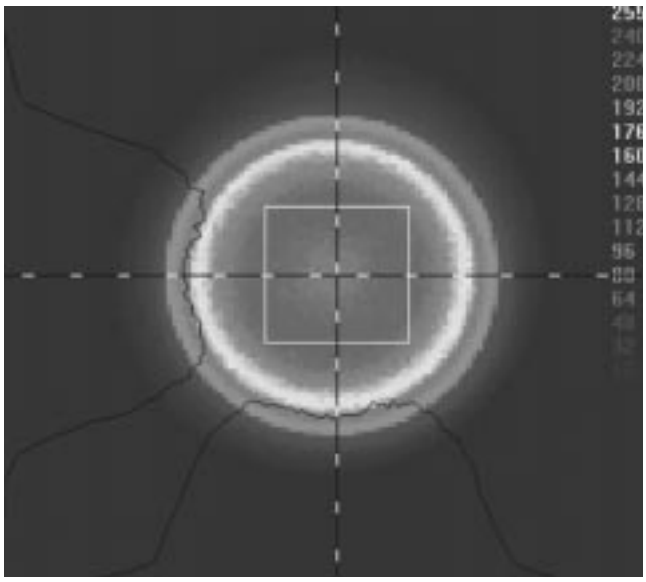

Fig. 18 Intensity profile of the laser beam used to illuminate cold particles in order to measure their flux, velocity, and size

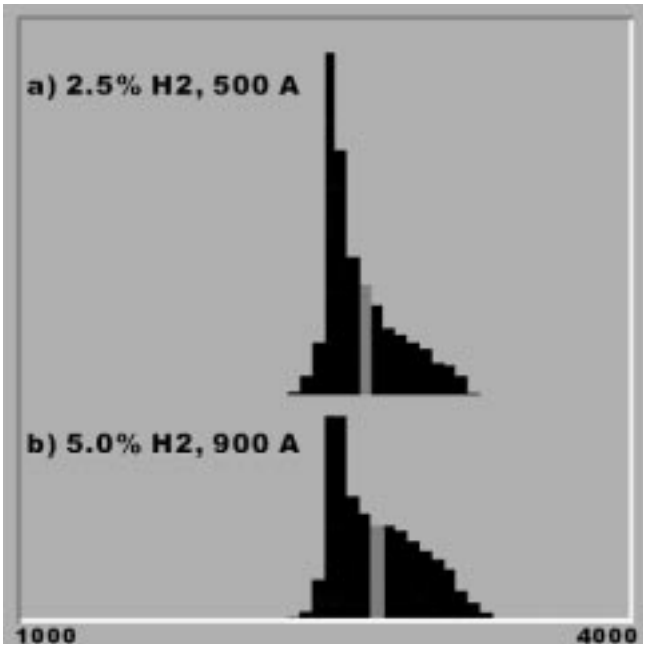

Fig. 19 Temperature distributions of yttria-stabilized zirconia powders during plasma spraying. The peak corresponds to the melting point of the material

resulting intensity profile of the laser beam is illustrated in Fig. 18. The laser diode wavelength matches the wavelength of one of the two branches of the DPV-2000 two-color pyrometer.

Results

Precise measurement of the particle temperature allows adjustment of the degree of melting of the particles during spraying. This might be of particular importance for depositing nanostructured materials to avoid excessive grain growth. Figure 19 illustrates an example of temperature distributions of yttria-stabilized zirconia powder during plasma spraying using two sets of spray parameters.[6] The peak appearing in both distributions corresponds to the melting point of this material at around 2700 °C. One sees that the amount of molten particles is significantly higher in Fig. 19(b) since the power and hydrogen flow rate are higher. With such information, it is possible to adjust the spray parameters to minimize the amount of superheated particles.

Particle monitoring is also useful to control HVOF processes. For example, recent studies showed that decarburation during spraying is related to the particle temperature, and coating porosity decreases with the particle velocity.[7,8]

Cold particle monitoring was performed with rounded molybdenum particles (32 to 45 microns) and angular iron oxide particles (38 to 45 microns) at room temperature. Results show that particle velocity and flux can precisely be measured regardless of particle size, shape, and temperature. Moreover, when particles are nearly spherical, precise diameter measurement can be achieved.

References

1. C.C. Berndt and E.J. Lavernia: *J. Thermal Spray Technol.*, 1998, vol. 7 (3), pp. 411-41.
2. E.J. Lavernia, M.L. Lau, and H.G. Jiang: in *Nanostructured Materials*, G.M. Chow and N.I. Noskova, eds., Kluwer Academic Publishers, 1998, pp. 283-301.
3. L. Pawlowski: *The Science and Engineering of Thermal Spray Coatings*, John Whiley & Sons, New York, NY, 1995.
4. Tecnar Automation Ltee, 3502 First Street, St-Hubert, PQ, Canada, J3Y 8Y5.
5. J. Blain, F. Nadeau, L. Pouliot, C. Moreau, P. Gougeon, and L. Leblanc: *Surface Eng.*, 1997, vol. 13, pp. 420-24.
6. L. Leblanc and C. Moreau: in *Thermal Spray: Meeting the Challenges of the 21th Century*, C. Coddet, ed., ASM International, Materials Park, OH, (1998) pp. 773-78.
7. L. Jacobs, M.M. Hyland, J. Gutleber, and S. Sampath: *United Thermal Spray Conf. Proc.*, E. Lugscheider and P.A. Kammer, eds., DVS, 1999, pp. 439-45.
8. B. Arsenault, P. Gougeon, J.G. Legoux, and C. Moreau: Surftec-Resources Progress Report #3, Industrial Materials Institute, National Research Council Canada, Nov. 1996.

22. Spectroscopic Measurements of DC-Arc Plasmas in Thermal Spray Processing Including Effects of Transverse Injection Jets

S.Y. Semenov and B.M. Cetegen
Mechanical Engineering Department, University of Connecticut, Storrs, CT 06269-3139
Contact e-mail: serg@engr.uconn.edu, cetegen@engr.uconn.edu

A complete and accurate knowledge of the plasma temperature field and its dependence on the plasma power and gas flow rates is a prerequisite for determining particle heat-up in plasma thermal spray processes. In particular, the effects of transverse particle injection jets on the plasma thermal field needs to be assessed for the many applications which utilize transverse injection. Due to the very high temperatures in the DC-arc plasma jets used in thermal spray processes, a spectroscopic technique was chosen to measure plasma temperatures based on the population of Ar-I species in different electronic states obeying a Boltzmann distribution. While such techniques had been used in the past,[1,2] our technique enables determination of plasma temperatures along a thin slice across the plasma width (or diameter) at one instant, thus allowing capture of the temperature profile along the chord. Because of the stable axisymmetric thermal field of the studied plasmas, Abel's inversion can be effectively used to remove the effects of line-of-sight integration.

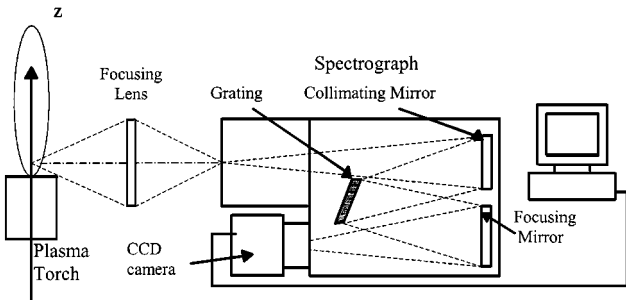

Fig. 20 Experimental setup

The experimental setup used for our measurements is schematically shown in Fig. 20. It images the plasma radiation using a single lens onto the entrance slit of a 0.5 m. McPherson spectrometer. The height of the spectrometer entrance slit covers the diameter of the imaged plasma, thus each location along the slit corresponding to a physical location along the plasma diameter. The spectrometer disperses the radiation across the slit width to its spectral content by using a 2400 grooves/mm diffraction grating. The spectrally dispersed radiation is then imaged at the output of the spectrometer using a high spatial resolution, scientific CCD camera. The spectral region spanned in these experiments covers 404 nm < λ < 435 nm, containing typically 10 emission lines belonging to Ar-I species. The image processing of the digital images from the CCD camera allows determination of the temperature at each radial location using the Boltzmann plot method.[3] Spectral sensitivity of the CCD chip is included in these calculations. Figure 21 shows the plasma emission spectrum for a 14.4 kW Ar-H_2 plasma using the Metco (mModel 9 MC) plasma system. It is found that the relative line

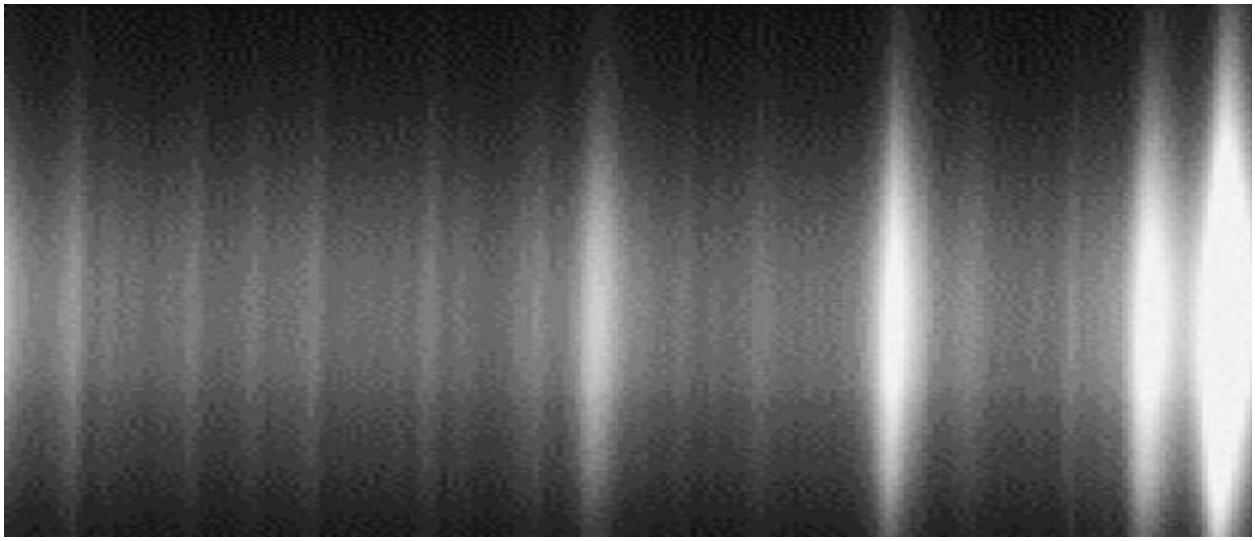

Fig. 21 Argon spectrum

intensities change from the center of the plasma (*i.e.*, the hottest core region) to its edges as expected. In contrast to the symmetric profiles obtained in undisturbed plasma shown in Fig. 21, the plasma thermal field with transverse gas jet impingement (as it would occur in transverse particle injection) becomes asymmetrical with the maximum temperatures shifting below the plasma torch axis.

This article will include results on the dependence of the temperature profiles on plasma power and gas flow rates. It is believed that the computational models used in calculating the particle heat-up must be checked against such new data to (1) gain confidence in the predicted thermal field and (2) calibrate the complex plasma prediction models to correctly predict the plasma temperature fields. These spectroscopic techniques can be extended to estimate the species composition to properly calculate thermal conductivities in these industrial plasma jets.

References

1. A. Vardelle, J. M. Barronnet, M. Vardelle, and P. Fauchais: *IEEE Trans. Plasma Sci.*, 1980, vol. PS-8 (4), pp. 417-24.
2. M. Vardelle, A. Vardelle, P. Fauchais, and M. I. Boulos: *AIChE. J.*, 1988, vol. 34 (4), pp. 567-73.
3. N. K. Joshi, S. N. Sahasrabudhe, K. P. Sreekumar, and N. Venkatramani: *Measurement Sci. Technol.*, 1997, vol. 8, pp. 1146-50.

23. CFD Simulation of Thermal Plasma Spraying of Nanostructured Ceramic Agglomerates

I. Ahmed and T.L. Bergman
Department of Mechanical Engineering, The University of Connecticut Storrs, CT 06269-3139
Contact e-mail: iahmed@engr.uconn.edu; tberg@engr.uconn.edu

Thermal spraying of micron sized metallic and ceramic powder particles on metallic substrates is a crucial part of some of the major material processing and manufacturing industries. Due to its ever increasing application as well as the widening range of properties demanded of the coatings thus produced, a deeper understanding of the process, its controlling parameters, and their specific effects on the end product is needed. A recent innovation in these processes has been attained through the use of agglomerated nanostructured ceramic as well as metallic carbide particles. It is believed that, in order to achieve the optimum deposition efficiency along with the maximum retention of nanostructure, a very narrow operating window will have to be identified and maintained throughout the spray process.

With this goal in view, the thermal plasma spraying process is being simulated using a commercial CFD package, FLUENT.[1] The plasma is simulated as a jet of a mixture of argon and hydrogen plasmas issuing into quiescent ambient air with the calculated transport properties at the relevant temperatures.[2] The "k–e" model along with the RNG extension is employed. The effects of the chemical reactions of the plasmas are not accounted for in these initial simulations. It may be noted that similar approaches have been adopted by a number of authors in modeling thermal plasma spray processes.[3,4]

Fully three-dimensional simulation of the plasma jet and plasma-particle interaction is made to investigate issues such as the transverse injection of particles, as well as that of carrier gas

injection. The CFD studies include the effects of the presence of a stationary target of the substrate material. The effects of random turbulent eddies have been included through a built-in feature of the FLUENT code.

The particles are modeled as spherical entities with constant properties, and the possibility of melting and resolidification are included. Since the focus of this study is agglomerated nanoparticles, which can be either solid or hollow (with a porous shell), all these attributes are considered, along with the variations in sizes.

Trajectories as well as temperature histories of particles of various sizes and porosities are predicted, along with the tracking of the solid-liquid fronts inside these particles. Stochastic predictions are made on sufficiently large numbers of particles in each group to obtain statistically meaningful results, and the results are analyzed in terms of both the distributions and their average values. One significant outcome of this study is the capability of predicting the fraction of nanostructure retained in agglomerates as a function of various operating parameters. These parameters include (1) particle size and porosity/hollowness, (2) plasma-gun to target stand-off distance, (3) plasma gun operating conditions, (4) effects of carrier gas, and (5) particle injection velocities and locations. In this work, we report the effects of some of these parameters. In addition to the particle state histories, the deposition locations on the target (from a stationary gun) are reported, and the variations in deposition spot size and its centroid, as a function of particle size/overall density, are also noted.

The obtained data agree quite well with those of similar experimental studies, albeit in a qualitative sense. But more importantly, some key issues are revealed through these initial simulations—such as the necessity to control the sizes of the injected particles and turbulence levels created inside the plasma gun, and the possibility of defining an optimum stand-off height for a given power level/plasma flow rate of the gun.

Together, these will allow one to predict the best conditions for spraying nanostructured particles that have a molten surface at impact and yet retain most of their nanostructure throughout their trajectories inside the plasma jet.

References

1. *FLUENT 4.4 User's Guide*, 2nd ed., Fluent Inc., Lebanon, NH, 1997.
2. B. Pateyron, M.-F. Elchinger, G. Delluc, and P. Fauchais: *Plasma Chem. Plasma Processing*, 1992, vol. 12 (4), pp. 421-48.
3. B. Dussoubs, A. Vardelle, and P. Fauchais: in *Progress in Plasma Processing of Materials*, Proc. 4th Int. Thermal Plasma Processes Conf., Athens, Greece, July 15-18, 1996, P. Fauchais *et al.*, eds., Begell House, New York, NY, 1997, pp. 861-69.
4. E. Lugscheider, C. Barimani, P. Eckert, and U. Eritt: in *Progress in Plasma Processing of Materials*, Proc. 4th Int. Thermal Plasma Processes Conf., Athens, Greece, July 15-18, 1996, P. Fauchais *et al.*, eds., Begell House, New York, NY, 1997, pp. 871-80.

24. Limitations of Fluid Models in Predicting the Splat Shapes of Nanosize Particle Impact

M. Pasandideh-Fard, J. Mostaghimi, and S. Chandra
Department of Mechanical & Industrial Engineering, University of Toronto, ON, Canada M5S 3G8
Contact e-mail: mostag@mie.utoronto.ca

Fluid models have been successfully used to predict splat shapes in thermal spray coatings. The dynamics of the impact phenomenon and the resulting shape of the splats as a result of (1) impact conditions, and (2) materials properties of both the powder and substrate materials have been successfully investigated by these models. To predict the dynamics of the impact, these models solve the Navier-Stokes equations along with the energy equation. In addition, the volume-of-fluid method is employed to predict the shape of the droplet during its impact. In this presentation, the limits of such models, in so far as the particle size is concerned, are examined. The limits are of two types: (1) numerical accuracy when the surface energy is a significant portion of the total energy; and (2) the limits of the continuum assumption, since the governing equations of the existing models make this assumption.

25. Numerical Simulations of a Metco HVOF Gun Used for *n*-WC/Co Coatings

S. Eidelman and D. Sharov
Science Applications International Corporation, McLean, VA 22102

Background

Coatings of nanoscale materials can be implemented using conventional HVOF equipment. However, due to small particle sizes, the physical and chemical properties of raw powder can differ significantly from the micron size material, and these can affect the gun operating condition required for optimal coating. Generally, the flow conditions have a stronger effect on nanoscale powders than on conventional powders, since the very small particle and low-density agglomerates will follow the streamlines very closely. The optimal conditions for nanopowder coatings can differ drastically from conventional powder coatings in terms of stand off distance, required jet temperature and velocity, and other conditions. Use of comprehensive nu-

merical simulation permits examination of the range of conditions that can affect plating of nanoscale materials and rapid process optimization, when used in conjunction with experimental study. Rapid analysis of the parametric space using numerical simulations will shorten the time for new coating development and allow better understanding of the parameters that control coating efficiency and quality.

Simulation Methodology

The thermal spray (TS) system analysis presented below is based on a comprehensive model of the HVOF TS system that numerically simulates:

- the gas dynamics of the gas expansion and flow in the barrel and in the free jet;
- particle injection and the interaction between the injected particle and the gas flow inside and outside the barrel; and
- particle interaction with the barrel walls.

The simulations are full 3-D to allow accurate implementation of geometrical details of the Metco gun, in particular, its eight burners. This capability is developed and validated for TS simulations. However, with some modifications, it can be used for high velocity impact fusion and plasma spray guns.

Simulation Results

We have simulated gas and particle flow of the Metco DJ-2700 gun with standard and with extended barrels. The cross section of the Metco DJ-2700 gun simplified geometry that was implemented in our simulations is shown as a CAD model in Fig. 22. This model was used for defining the numerical grid over the computational domain. The computational domain was designed to focus on simulation of the particle and gas flow in the combustion chamber, nozzle, and expanding jet.

For the Metco DJ-2700 gun, a 3-D simulation is required since an axisymmetric assumption can not describe the eight jets of the burning propylene/oxygen mixture. The computational domain is discretized using a tetrahedral grid shown in Fig. 23. The chemical state of the gas flow in the barrel can be considered to be in equilibrium or have a frozen composition. Experi-

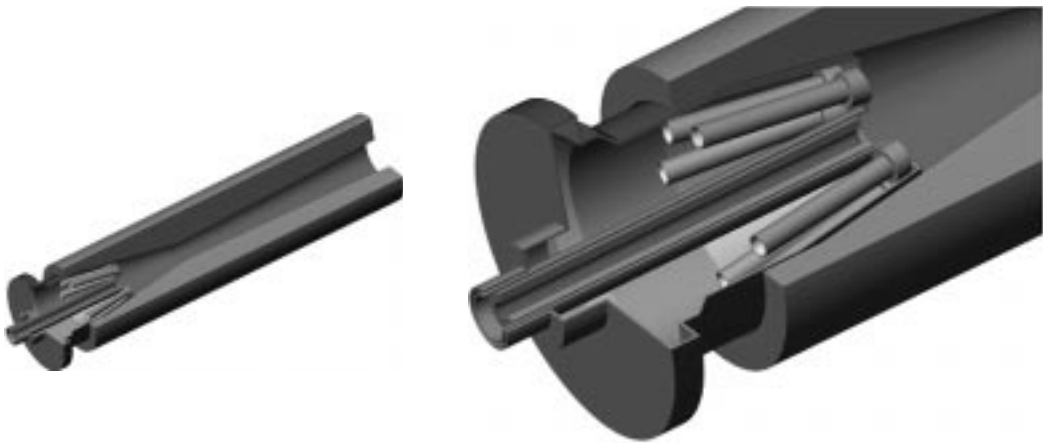

(a) **(b)**

Fig. 22 CAD model of Metco-2700 gun. (**a**) General view and (**b**) injection region close-up

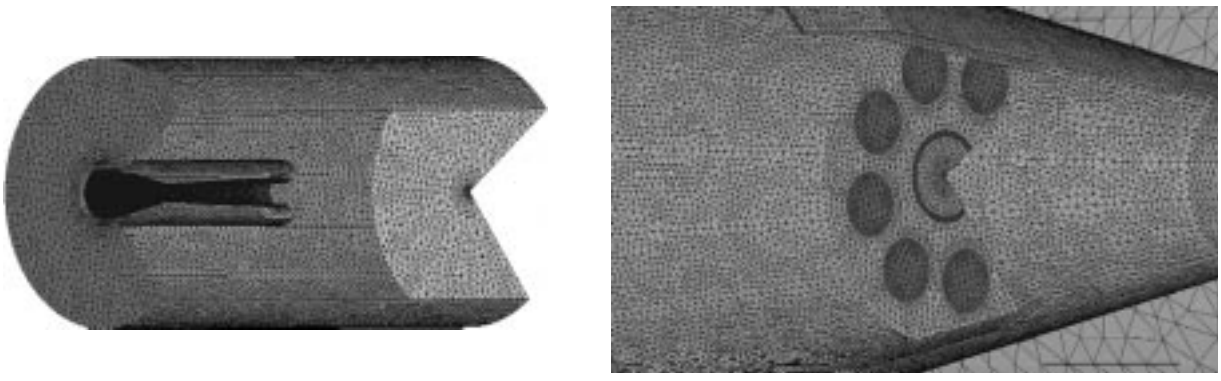

(a) **(b)**

Fig. 23 Computational domain decomposition by tetrahedral grids. (**a**) General view and (**b**) injection area close-up

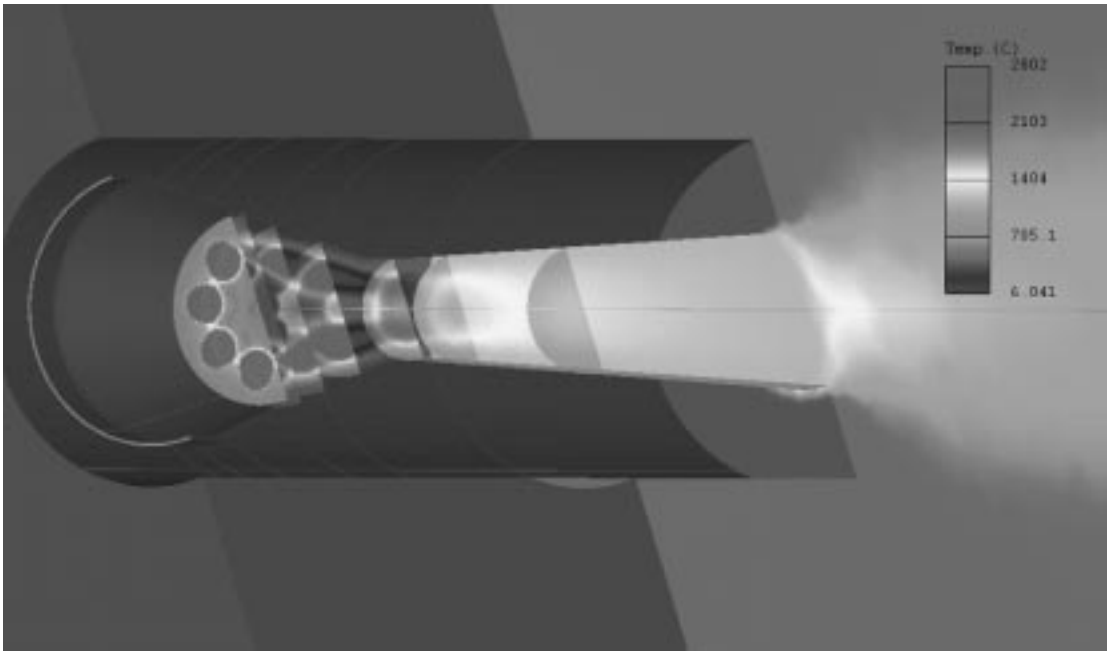

Fig. 24 Gas temperature in the barrel and jet area

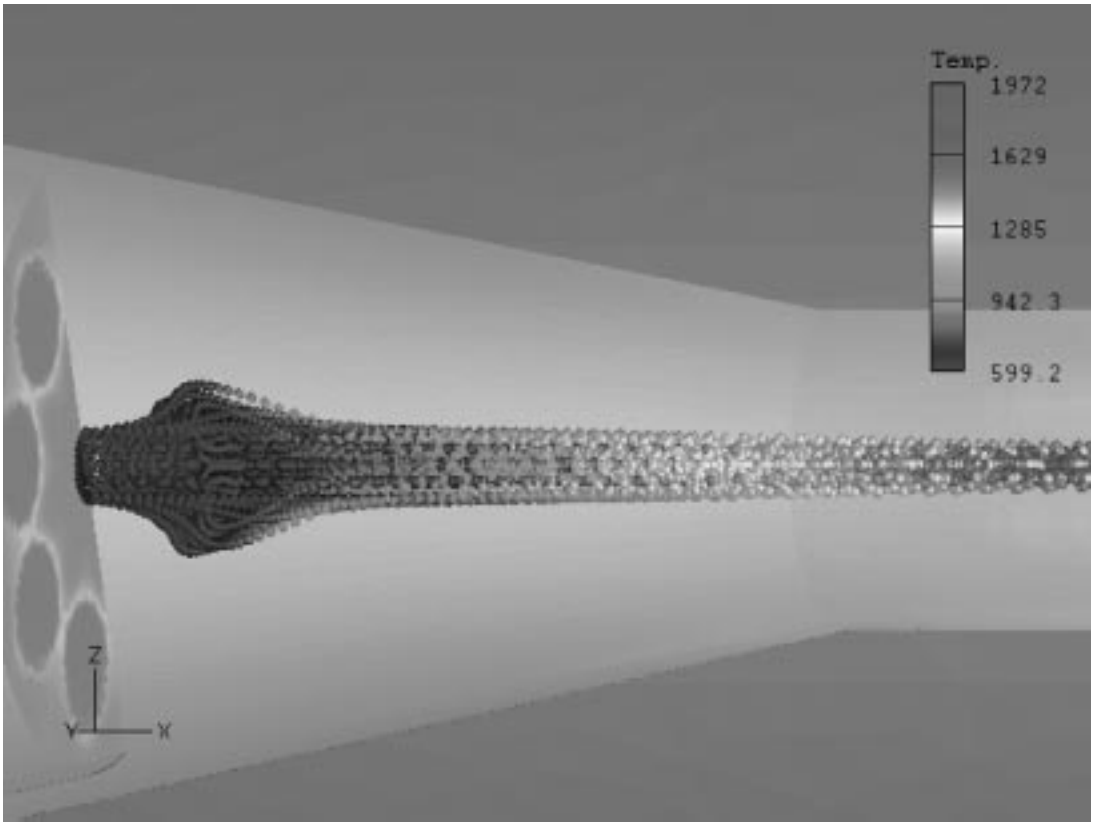

Fig. 25 Particle flow in Metco DJ-2700 gun. Injection and nozzle area

mental measurements also indicate that the flow is closer to the frozen state than equilibrium. This is because the gas residence time is shorter than the chemical reaction time. Thus, we assumed in our simulations that the gas has a frozen chemical composition for a given fuel/oxygen ratio. The state of gas in a frozen condition can be calculated using the NASA Gordon-McBride program. We simulated the Metco DJ-2700 gun flow for the following flow conditions: propylene mass flow: 176 scf/h; oxygen mass flow: 578 scf/h; air mass flow: 863 scf/h; nitrogen mass flow: 29 scf/h; and ambient air conditions: T = 300 K, P = 101,325 Pa.

Given these conditions and the gun/barrel geometry, we simulated the steady-state flow regime for the flow generated by the gun and particle flow. We considered particle flow of *n*-WC/Co powder. A sample of simulation results to be presented is shown in Figs. 24 and 25 in the form of particle and gas flow in the gun barrel and jet areas. In Fig. 25, particles are shaded according to their temperature.

26. Precipitation Phenomena in Nanostructured Cr_3C_2-NiCr Coatings

Jianhong He, M. Ice, and E.J. Lavernia
Department of Chemical and Biochemical Engineering and Materials Science
University of California, Irvine, CA 92697-2575

Precipitation phenomena in thermally sprayed nanostructured Cr_3C_2-NiCr coatings were investigated in detail. The results show that microhardness of the conventional coating increased only slightly with an increase in the exposure temperature, whereas that of the nanostructured coating increased from 1020 to 1240 DPH_{300}. Compared with the conventional Cr_3C_2-NiCr coatings, the scratch resistance and coefficient of friction were found to increase and be reduced, respectively, in the nanostructured coatings.

The observed increases in microhardness and scratch resistance and decrease in coefficient of friction of the nanostructured coatings are attributed to a high density of oxide nanoparticles precipitaing within the coating as the exposure temperature increases. In addition to the precipitation of oxide particles, the changes in the as-sprayed NiCr amorphous phases of the nanostructured coatings exposed to elevated temperatures were examined. The amorphous structure crystallized during thermal exposure and thin deformed twins developed. There was no evidence indicating the presence of precipitates in the original NiCr amorphous phases.

27. The Effect of Powder Processing Method on the Physical Properties of Nanocomposite WC-Co Thermally Sprayed Coatings

A.H. Dent, S. Sampath, and H. Herman
Center For Thermal Spray Research, State University of New York, Stony Brook, NY 11794-2275
Contact e-mail: adent@ctsr.eng.sunysb.edu

Unique chemical processing advances in the production of WC-Co (cermet) powders has led to the development of composite powder particles that contain nanoscale (sub-micron sized) WC second phase grains. Research on the effect of carbide size in thermally sprayed WC-Co cermets produced by conventional methods (incorporation of carbide particles of a pre-determined size into a Co binder) has shown that, in general, wear properties deteriorate as the carbide size is reduced.[1] However, improved hardness and tool life values of sintered cermet components using nanograin carbides over conventional (5 to 8 m) sized carbides have led to interest in the properties of thermally sprayed coatings using these unique materials.

HVOF spraying using a Metco DJ2700 system (propylene fuel gas) was used to deposit four submicron carbide cermets as well as a conventional cermet powder. These powders and their production methods are listed in Table 2. X-ray diffraction (XRD) traces of the resultant coatings (Fig. 26) show that there is a wide variation in the decomposition of the WC phase: in general, the larger the average WC particle, the greater the degree of degradation (XRD analyses of all the as-received powders revealed a mixture of WC and crystalline Co). Also worth noting is the almost complete loss of WC within coating D compared to coatings A and B, which have equivalent WC particle sizes. XRD analyses of A and B show that an increase in the proportion of Co binder phase within the powders produced by the solutionizing method did not significantly alter the degree of decomposition of WC. This would suggest that the degradation of WC within material D is likely to be the result of powder processing. Coating E shows very little formation of W_2C, typical of sprayed agglomerated and densified powders deposited by HVOF.[2]

Diagnostic temperature and velocity measurements in flight are presented in Table 3. It is clear that the severe degradation of powder D was not a result of higher in-flight temperatures; in fact, the material with the lowest decomposition (E) attained the highest temperatures within the flame. Splat morphologies from these materials also revealed large differences in the way the materials were deposited. Average splat sizes for material D were found to be almost half that seen for the other four deposits (Fig. 27), despite similar as-received powder particle sizes; see Table 2. The actual splat sizes suggest that material D either suffered disintegration of the particles in-flight or the larger powder particles did not adhere to the substrate. The reduction in Co content between materials B and A did not result in significant changes in the splat morphologies.

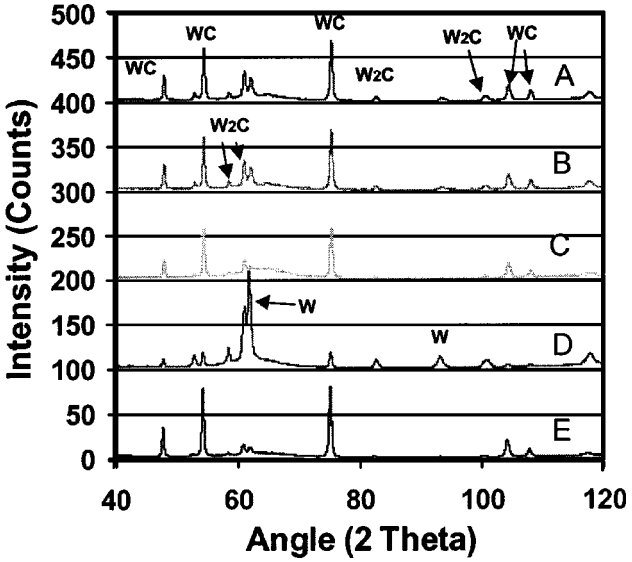

Fig. 26 XRD analysis for the five coatings tested

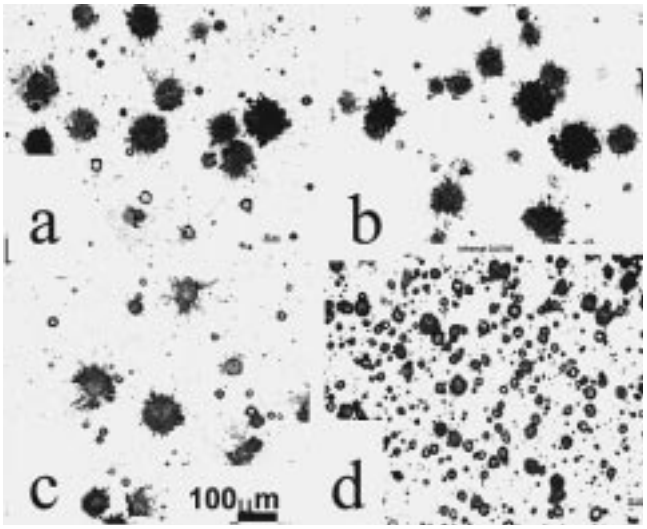

Fig. 27 Multiple splat morphologies on polished steel for coatings A, B, C, and D in a, b, c, and d, respectively

Table 2. Compositions, size distributions, and processing routes for the materials deposited

Material	Manufacturer	Approximate WC size	Wt.% Co	Processing	Size distribution
A	Nanodyne	20–200 nm	8	Spray conversion processing	–113 + 18 lm
B	Nanodyne	20–200 nm	15	Spray conversion processing	–110 + 11 lm
C	Osram Sylvania	Less than 1 lm	18	Spray dried/sintered	–53 + 5 lm
D	Inframat	20–200 nm	8	Reproced from nanodyne WC-8% Co	–41 + 10lm
E	Praxair	0.75–5 lm	17	Spherodized/densified	–53 + 15.lm

Table 3. Diagnostic measurements and wear data for materials A to E*.

	Material				
	A	B	C	D	E
Temperature	1888 ± 146	1790 ± 164	1767 ± 151	1952 ± 196	2079 ± 152
Velocity	656 ± 102	644 ± 89	637 ± 85	670 ± 96	554 ± 76
Abrasion	181.3 (std. dev. 57.2)	148.2 (std. dev. 49.9)	272.5 (std. dev. 76.7)	273.0 (std. dev.58.9)	49.0 (std. dev. 6.2)
Erosion	0.03228	0.03128	0.03738	0.03391	0.01605

*Weight loss measurements due to abrasion were averaged over six coating specimens, and weight loss measurements due to erosion were averaged over 3 specimens. The media for the abrasion and erosion tests were SiC and 50 μm Al_2O_3, respectively

High resolution scanning electron microscopy (SEM) of the coatings corroborated evidence from XRD with a higher degree of degradation of the WC particles in the submicrometer WC coatings (A–D). Severe rounding of the WC particles was observed for coating D, suggestive of greater particle dissolution.

Averaged results from 3-body abrasion, and erosion testing of the coatings are also shown in Table 3. Weight loss due to erosion at 90° was found to be greater for the coatings with smaller average carbide particles, the most resistant being coating E. Three-body abrasion followed the same trend, with the conventional sized WC particle powder providing the greatest wear resistance. Variations in Co content for the nanostructured carbides (A and B) showed an improvement in wear resistance for higher Co; however, weight loss was still considerably higher than for the conventional WC sized material (D).

Powder processing routes for nanostructured WC-Co materials clearly play a critical role in the formation of these cermet coatings using HVOF. Further examination of deposition processing optimization is also essential for the development of improved properties of these promising materials.

Acknowledgments

The authors acknowledge support from the Office of Naval Research Grant No. N000149910405. The use of facilities through the MRSEC program of the NSF under Award No. 96-32570 is also acknowledged.

References

1. S. Usmani, S. Sampath, D. Houck, and D. Lee:, *Tribol. Trans.*, 1997, vol. 40 (3), (1997) pp. 470–78.
2. C.-J. Li, A. Ohmori, and Y. Harada: *J. Mater. Sci.*, 1996, vol. 31, pp. (1996) 785–94.

28. Fatigue Behavior of Nanostructured and Conventional Coatings

R.L. Holtz and K. Sadananda
Naval Research Laboratory, Washington, DC 20375

Fatigue failures of coated substrates can occur in the coating itself, at the coating-substrate interface, or in the substrate. In applications where coating damage is caused primarily by surface contact, such as wear resistant and rolling contact coatings, high-cycle fatigue of the coating and interface is less likely to be a failure mode of much concern. In other applications such as thermal barrier and corrosion resistance coatings, fatigue of the coating and interface can be a principal failure mode. Regardless of the coating application, fatigue of the substrate is always a concern and it is important to understand the effect of a coating on substrate fatigue.

Of particular interest is the fatigue of nanostructured coatings compared to conventional grain size coatings. There has been very little research published on the fatigue of nanostructured materials. In conventional materials, a simple argument for grain size effects is that the grain size scale for fatigue threshold behavior is comparable to the size of the reverse plastic zone under tensile stress.[1] This leads to the simple result that the cyclic fatigue threshold stress intensity ΔK_{th} is proportional to the yield strength times the square root of the grain size, $\Delta K_{th} \propto \sigma_y d^{1/2}$. If the yield strength exhibits Hall-Petch behavior, $\sigma_y = \sigma_{y0} + k/d^{1/2}$, the net result is that the fatigue threshold should decrease with decreasing grain size. Accounting for change of deformation behavior[2] from dislocation to grain boundary sliding mechanisms suggested by anomalous or inverse Hall-Petch behavior exhibited by nanostructured materials at grain sizes below 30 nm or so, the threshold would decrease even faster with decreasing grain size. This argument consequently suggests that for given stress intensities, nanostructured materials would tend to have lower thresholds and higher fatigue crack propagation rates than larger grain size materials.

In nanostructured FeMoSiB alloys, it has been observed that the fatigue limit behaves similarly to the ultimate tensile strength, showing a peak for grain sizes around 40 nm but decreasing for smaller or larger grains.[3] This suggests that while the fatigue limit may be enhanced, fatigue cracks, once formed, may tend to propagate faster in nanostructured compared to conventional grain-sized materials. In addition, fracture toughness of nanostructured WC-Co[4] may be much lower than conventional grain size materials, so that unstable crack growth might set in at lower stress intensities in nanostructured materials.

Fatigue of a coating-substrate interface can take two main forms—debonding of the coating from the substrate, or if the bond strength is very high, fatigue cracking due to normal plastic slip processes in ductile layers adjacent to the interface.[5] In many cases, fatigue damage of the interface is a consequence of failures in either the substrate or coating.[6] In instances where debonding is more favorable than slip for stress relief at the interface, cracks originating in the coating can deflect into the interface. For strongly bonded coatings, cracks originating in the coating can propagate into the substrate, and *vice versa*. Therefore, if fatigue life of the substrate is more critical than coating integrity, high bond strength is not necessarily beneficial. In addition, stress concentrations in a strongly bonded coating become critical to the fatigue life because they act as crack initiation sites.

A very important problem is the effect of the coating on the fatigue of the substrate due to the coating. Compressive stresses in a coating transmit tensile stress to the substrate surface. These tensile stresses superimpose on any applied stresses, resulting in larger net tensile stress at the substrate surface and this causes enhanced crack initiation and growth rates. For example, WC-Co coatings with compressive residual stress thermally sprayed onto aluminum and steel have been found to decrease fatigue life by over a factor of 30.[7] Strangely, higher compressive residual stress apparently reverses this degradation, returning the fatigue life to values comparable to an uncoated substrate. It is possible that other failure mechanisms such as spalling and microcracking in the high-stress coatings may act to relieve the stress at the interface; *i.e.*, damage to the coating helps preserve the substrate. In any case, it is clear that internal stress in the coating, which can be very sensitive to processing conditions, can have significant impact on fatigue of the substrate. In particular, a low-compressive residual stress coating is not necessarily beneficial for fatigue life, although it may extend coating life.

Nanostructured coatings may have less effect on the fatigue life of a substrate than larger grain-sized materials because high creep rates of nanostructured materials should act to relieve residual stresses. Diffusional creep is proportional to the inverse second power of the grain size and dislocation creep is proportional to the inverse third power of grain size in conventional grain-sized materials. Therefore, in general, creep is expected to increase with decreasing grain size. Enhanced grain boundary diffusional creep (Coble creep) has been predicted to become the dominant mechanism below a critical grain size because the relative fractions of grain boundary and bulk material increase with decreasing grain size.[8,9]

The relative roles of fatigue mechanisms of nanostructured versus conventional coatings, and the different coating processes on fatigue behavior, are being studied and results will be discussed. Experimental results of fatigue life measurements using a four-point bend test technique on thermal spray coated WC-Co on various substrates will be presented.

References

1. S.D. Antolovich: *ASM Handbook*, vol. 19, *Fatigue and Fracture*, ASM International, Materials Park, OH, 1996, p. 37.
2. H. Hanh, P. Mondal, and K.A. Padmanabhan: *Nanostr. Mater.*, 1997, vol. 9, pp. 603-06.
3. S. Li, K. Lu, F. Guo, R. Chu, and Z. Wang: *Mater. Lett.*, 1997, vol. 30, pp. 305-10.
4. K. Jia, T.E. Fischer, and B. Gallois: *Nanostr. Mater.*, 1998, vol. 10, pp. 875-91.
5. M.C. Shaw, D.B. Marshall, B.J. Dalgleish, M.S. Dadkhah, M.Y. He, and A.G. Evans: *Acta Metall. Mater.*, 1994, vol. 42, pp. 4091-99.
6. A.G. Evans and J.W. Hutchinson: *Acta Metall. Mater.*, 1995, vol. 43, pp. 2507-30.
7. R.T.R. McGrann, D.J. Greving, J.R. Shadley, E.F. Rybicki, T.L. Kruecke, and B.E. Bodger: *Surface Coating Technol.*, 1998, vol. 108-109, pp. 59-64.
8. S. Shah and A.H. Chokski: Coll. Surfaces A, 1998, vol. 133, pp. 57-61.
9. N. Wang, Z. Wang, K.T. Aust, and E. Erb: *Acta Metall. Mater.*, 1995, vol. 43, pp. 519-28.

29. Structure/Property Relationships and Barrier Performance of Thermally Sprayed Nanoreinforced Polymer Coatings

E. Petrovicova, R. Knight, F. Xiaohua, and T.T. Twardowski
Department of Materials Engineering, Drexel University, Philadelphia, PA
Contact e-mail: knightr@drexel.edu

L.S. Schadler and T. Hanlon
Materials Science and Engineering Department, Rensselaer Polytechnic Institute Troy, NY

Thermal spray has previously been shown to be an excellent solution for processing nanoreinforced polymer/ceramic composites as coatings.[1, 2] Since it eliminates the need for solvents, processing is not limited by the viscosity of the melt, and large surfaces can be coated in the field. Dense coatings have been produced using HVOF combustion spraying through careful control of the particle dwell time in the jet and substrate thermal management. Consistent, uniform dispersion and distribution of the reinforcing nanoparticulates within the polymer matrix is the primary processing challenge and has been shown to have a significant influence on the properties of the resulting coatings. Results have shown that nanoreinforced nylon 11/silica coatings (with nominal silica contents of 5 to 15 vol.%) exhibited improved mechanical properties (dynamic modulus), scratch and sliding wear resistance; depending both on optimum filler dispersion and on coating morphology, including changes in crystallinity.

These nanocomposite coatings also exhibited decreased water vapor permeability compared to pure polymer coatings. Coatings produced from smaller (30 μm mean particle size) nylon 11 powders (designated "D-30") were found to be denser than those produced from coarser nylon 11 powders (60 μm

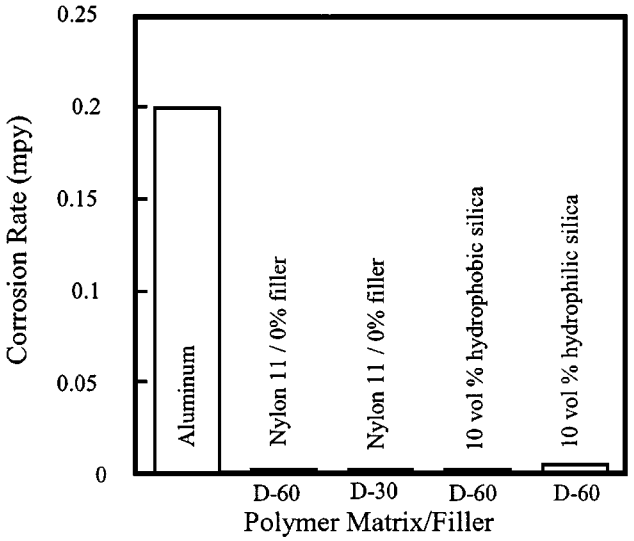

Fig. 28 Corrosion rates of Al substrates coated with nylon 11 D-30 and D-60 with different types of nanosized silica filler (no presoak)

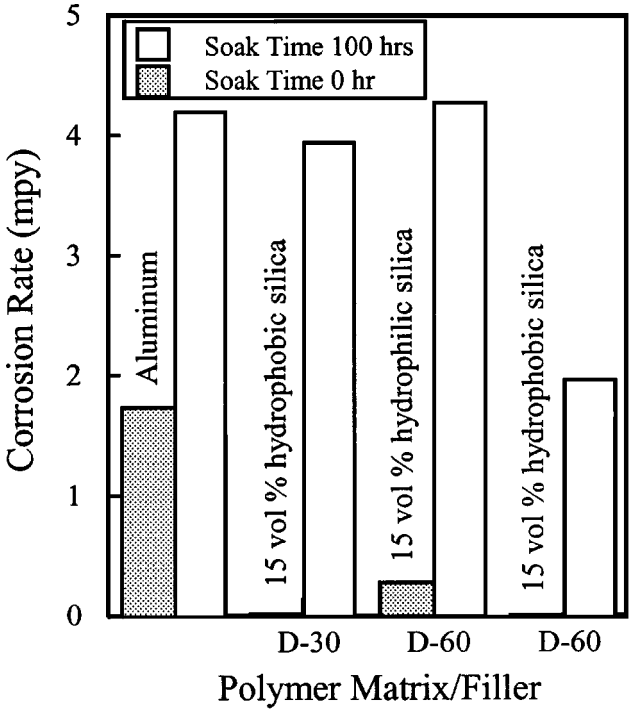

Fig. 29 Corrosion rates of Al substrates with intentional damage and two soak times

mean particle size, designated "D-60") for the same filler content. Smaller feedstock particles were believed to have been heated more homogeneously, thus improving polymer flow on impact; resulting in improved filling of the interstices between particles and denser coatings. While the original crystallites in the smaller size powder particles were believed to have been fully remelted during spraying, the high cooling rates typical of thermal spray processes resulted in deposits with lower crystallinity contents. Improvements in the mechanical properties of the D-30 materials were comparable to those for D-60 at lower filler contents (5 vol.%) but did not reach the values exhibited by the D-60 at 15 vol.% filler. These results are likely related to the lower crystallinity content observed for the D-30 coatings compared to the D-60 deposits. Coating density/porosity was found to be the dominating factor affecting barrier properties.

The improved mechanical and barrier properties of thermally sprayed nanocomposite coatings, together with the versatility of thermal spray deposition, indicated significant potential applications for these coatings for the corrosion protection of large metallic surfaces where increased wear and scratch resistance are required. Electrochemical impedance spectroscopy (EIS) testing (a detailed description of the method is contained in Ref 3) showed that thermally sprayed polymer/ceramic nanocomposite coatings can effectively protect metallic substrates against corrosion. As-sprayed nanocomposite coatings on Al substrates and coatings with defects introduced intentionally using a Rockwell hardness tester ball have been tested to more closely represent actual service conditions. Coatings were submerged in a 0.5 M NaCl solution and the corrosion rates evaluated for 0 and 100 h soak times.

The corrosion rate of samples coated with pure polymer D-60 and D-30 coatings and polymer D-60 with 10 vol.% silica fillers exhibited high corrosion resistances compared to the uncoated aluminum substrate (Fig. 28). Figure 29 indicates that the absence of presoaking coatings with intentionally introduced defects also exhibited higher corrosion resistances than the aluminum substrate. After coated samples were subjected to a prolonged soak in NaCl, however, crevice corrosion was observed and the rate of corrosion increased. Small differences in corrosion rate were observed between coatings filled with hydrophobic and hydrophilic silica fillers, similar behavior to that observed for permeability. These may have been due to differences in adhesion and/or coating permeability, or due to the presence of defects such as porosity. Future testing will concentrate on evaluating the influence of these effects on the corrosion performance of the coatings.

References

1. L.S. Schadler, K.O. Laul, R.W. Smith, and E. Petrovicova: *J. Thermal Spray Technol.*, 1997, vol. 6 (4), (1997) pp. 475-85.
2. E. Petrovicova, R. Knight, R.W. Smith, and L.S. Schadler: *Proc. 1st United Thermal Spray Conf.*, ASM International, Indianapolis, IN, 1997, pp. 877-83.
3. F. Mansfeld: *Corrosion*, 1981, vol. 36 (5), pp. 301-07.

30. Comparative Study of Wear Behavior of Coatings Made from Nanostructured and Commercial Powders

D. Goberman, L.L. Shaw, and M. Gell
Department of Metallurgy and Materials Engineering, University of Connecticut Storrs, CT 06269

Nanostructured coatings can provide significant improvements in wear and erosion resistance deriving from enhanced hardness and toughness. In this study, the tribological behavior of thermally sprayed Al_2O_3-13 wt.% TiO_2 coatings on steels using nanosized Al_2O_3 and TiO_2 powder feeds was investigated

Table 4. Summary of thermal spray conditions, phase content, indentation crack length, and microhardness of various coatings

ID(a)	Nozzle	I.V/Ar	γ/α(b)	Crack length	HV_{300}
N194	GH	325–350	2.33	0.25 mm	1070 ± 110
N195	GH	298	1.85	0.16 mm	1080 ± 127
N198	GP	298	1.66	0.25 mm	988 ± 117
M199	GH	290–312	4.80	0.31 mm	1195 ± 84

(a) N and M in the sample ID refer to nanocoating and Metco-130 coating, respectively
(b) γ/α stands for the ratio of γ- to α-Al_2O_3 phases in the coatings estimated *via* the intensity ratio of the XRD peaks.

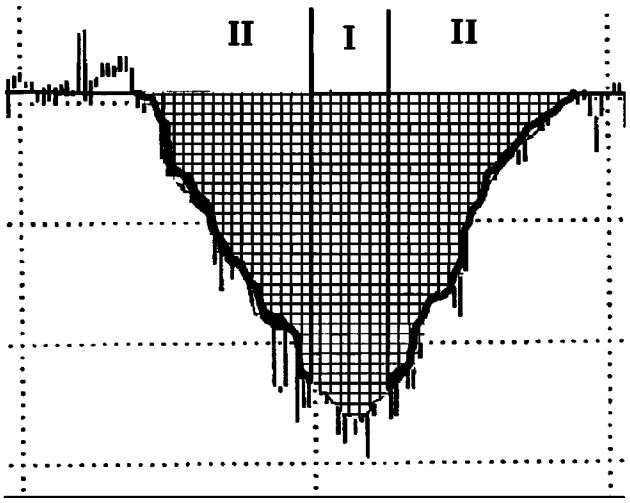

Fig. 30 Typical contour of the wear track determined using a profilometer

and compared with that of thermally sprayed coatings of the same composition but using commercial powder (Metco 130) as feedstock. A variety of analytical techniques including x-ray diffraction (XRD), scanning electron microscopy (SEM), transmission electron microscopy (TEM), and profilometry were used to determine the phase content, grain size, microstructure, and wear mechanisms of these oxide coatings. The hardness and toughness of the coatings were also determined. Efforts were made to relate the wear behavior of different coatings to their microstructures and basic mechanical properties such as hardness and toughness. The key material parameters that influence wear behavior of these coatings were proposed.

It was found that thermal spray conditions have immense influence on the microstructure, hardness, density, and phase content of the oxide coatings. The detail of these influences can be found elsewhere.[1] Among various thermal spray parameters, the ratio of the electrical power (I.V) to the primary Ar gas flow rate, denoted as I.V/Ar hereafter, has the most influential effect on the microhardness and density of the coating. Typically, the microhardness of the coating increases with the I.V/Ar ratio.[1] Thus, in this study, we have selected two I.V/Ar ratios to thermally spray oxide coatings. The I.V/Ar ratio and nozzle used to spray these coatings are summarized in Table 4. Included are also the microhardness, indentation crack length, and the ratio of γ- to α-Al_2O_3 phases in the coating. It can be seen that sample M199 sprayed using Metco 130 powder exhibits the highest microhardness and γ- to α-Al_2O_3 ratio, but the lowest crack propagation resistance. In contrast, sample N195 exhibits the highest crack propagation resistance. It also contains a high volume fraction of α-Al_2O_3 in comparison with N194 and M199 samples.

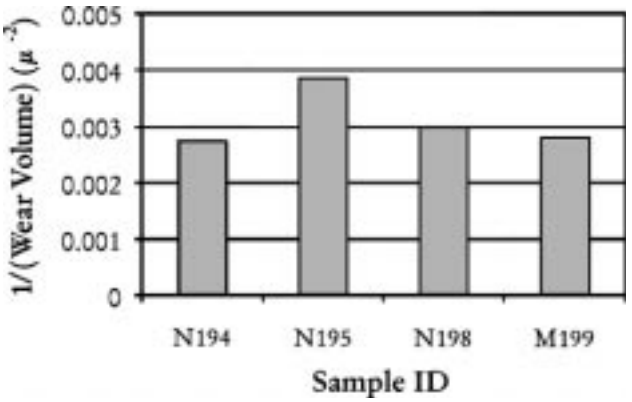

Fig. 31 Sliding wear resistance of Al_2O_3-13 wt.% TiO_2 coatings

A typical contour of the wear track of the oxide coatings sliding against a Si_3N_4 ball determined using a profilometer is shown in Fig. 30. The hatched area is where the wear track is located. The integration of this hatched area is proportional to the wear volume loss of the oxide coating, and, therefore, the reciprocal of the hatched area represents the wear resistance of the coating. A summary of the wear resistance of various coatings based on this parameter is presented in Fig. 31. It can be seen that sample N195 provides the best wear resistance among the samples investigated.

Examination of the wear track surface using SEM provides some insights into why N195 sprayed using nanopowder feeds has a better wear resistance than Metco 130 coating (M199). Figure 32 shows the wear track surface of N195 before and after ultrasonic cleaning. Before ultrasonic cleaning (Fig. 32a), the wear track surface is covered with a thin layer of fine particles with sizes from 30 to 300 nm. Region B in the figure contains even finer particles when examined under higher magnifications. These particles are believed to be wear debris because this fine particle layer disappears after ultrasonic cleaning (Fig. 32b). Such a thin layer of fine particles is found to be present at most of the wear track surface, located at region II as defined in Fig. 30.

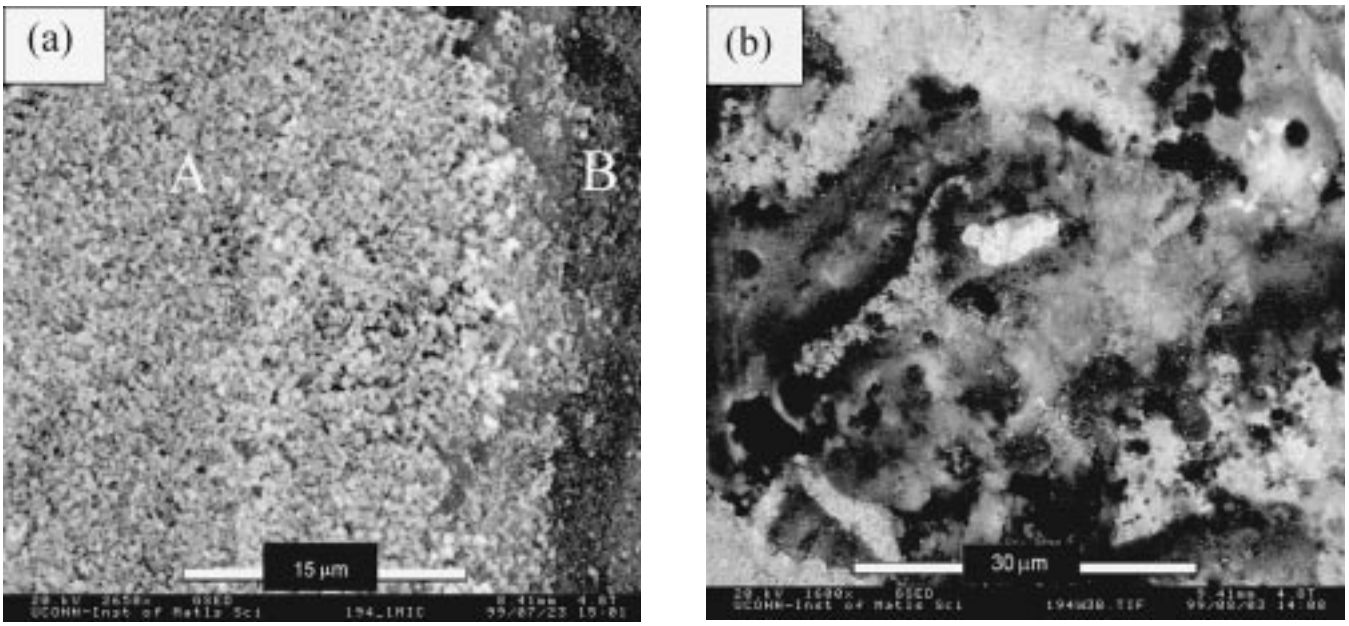

Fig. 32 Wear track surface of N195 sliding against a Si_3N_4 ball under a force of 4.9 N with 20,000 rotations: (**a**) before and (**b**) after ultrasonic cleaning

However, the bottom of the wear track (*i.e.*, region I in Fig. 30) does not have such a thin layer of fine particle debris, but exhibits the morphology similar to that shown in Fig. 32(b). The absence of fine particle debris at region I is probably due to the large contact stress there. This large stress pushes debris to region II. The presence of this thin layer of wear debris particles suggests that the wear mechanism of nanocoatings is associated with intergranular and/or transgranular fracture of the oxide coatings. Thus, sample N195 should have the best wear resistance since it has the highest fracture resistance among all the samples studied. The present data also seem to suggest that hardness is not critical in determining wear resistance when the microhardness has reached about 1000 kg/mm^2. More detailed studies are currently under way to further investigate this issue.

References

1. L. Shaw, D. Goberman, M. Gell, S. Jiang, Y. Wang, T.D. Xiao, and P. Strutt: *SurfaceCoatings Technol.*, 2000, vol. 130 (1), pp. 1-8.

31. Hypersonic Plasma Particle Deposition of Nanostructured Silicon Carbide Films for Friction and Wear Resistance

N. Tymiak and W. W. Gerberich
Department of Chemical Engineering and Materials Science, University of Minnesota, Minneapolis, MN 55455

J. Blum, A. Neuman, N.P. Rao, P.H. McMurry, J.V.R. Heberlein, and S.L. Girshick
Department of Mechanical Engineering, University of Minnesota, Minneapolis, MN 55455

We have developed a new method for depositing nanostructured coatings, known as hypersonic plasma particle deposition (HPPD). In this method, gaseous reactants are injected into a thermal plasma, which is then expanded through a nozzle, with the pressure dropping from slightly subatmospheric to about 2 Torr. The resulting sharp temperature drop in the nozzle drives the nucleation of nanoparticles, which issue into the low-pressure expansion and are accelerated by the highly supersonic flow. These particles are then inertially deposited on a substrate positioned perpendicular to the flow and form a nanostructured coating.

HPPD can be considered a plasma spray method, in that nanoparticles are sprayed onto a substrate. However HPPD differs from conventional plasma spray, in that these particles are not injected as a powder into the spray torch—particles this small would quickly evaporate—but rather are nucleated downstream of the hot plasma, in the nozzle expansion. The motivation for operating the expansion in the hypersonic regime is that this allows the critical particle size for inertial deposition to be as small as a few nanometers.[1] In contrast to "soft landing" deposition modes such as diffusion, thermophoresis, or gravitational settling, inertial impaction may provide at least a preliminary ballistic consolidation of the deposited material. An additional benefit of HPPD is that it minimizes the in-flight formation of hard agglomerates because the residence time from the nozzle exit to the substrate is on the order of 100 μs, too short for significant coagulation to occur.

We have used HPPD to deposit silicon carbide films at rates on the order of a few tenths of a micron per second with complete coverage over a 2 cm diameter molybdenum substrate.[2–4] Silicon carbide was synthesized by injecting silicon tetrachloride and methane into an argon-hydrogen plasma. Deposited films were characterized by a variety of techniques, including scanning and transmission electron microscopy, micro-x-ray diffraction (XRD), Raman backscattering spectroscopy (RBS), and micro- and nanoindentation. The film grain size was typically about 20 nm, corresponding closely to particle size measurements obtained by sampling the aerosol jet and measuring the particle size distribution with a scanning electrical mobility spectrometer. Substrate temperature, which was varied over the range 250 to 700 °C, did not appear to affect the grain size, indicating that minimal grain growth occurred during the deposition. This may be attributable to the short deposition times, typically about 1 min. Elemental composition determined by RBS indicated that these films were close to stoichiometric SiC, and that chlorine content ranged from 8.5 to 1.5 at.% as substrate temperature ranged from 450 to 700 °C. Film density as determined by RBS ranged from 74 to 80% of the theoretical density of SiC, indicating that significant ballistic consolidation had indeed occurred.

Substrate temperature was found to influence several other properties of the deposits. At lower temperatures, the deposits consisted of amorphous silicon carbide, whereas for substrate temperatures around 700 °C the deposits were mainly crystalline β-SiC.

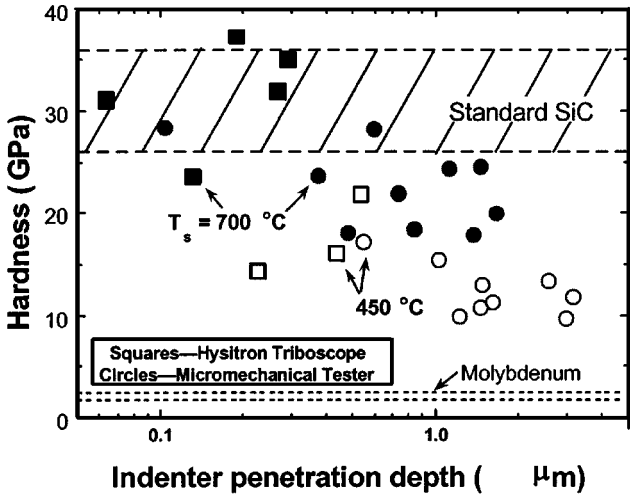

Fig. 33 Measured hardness vs nanoindenter penetration depth of two silicon carbide films deposited at a substrate temperature of either 450 or 700 °C

XRD also showed that a molybdenum carbide interlayer formed in the higher-temperature deposits, but not for the lower substrate temperatures, and this appeared to promote film adhesion.

Film hardness was characterized with micro- and nanoindentation techniques. Figure 33 shows hardness measurements obtained from nanoindenter load-displacement curves for two films deposited at substrate temperatures of either 450 or 700 °C. Two different instruments were used: a Hysitron Triboscope, with an indenter having a 90° cone and 400 nm tip radius, which operates in the small-load (≤15 mN), small-penetration-depth regime; and a Micro-mechanical Tester, whose indenter has a 90° cone and 1 μm tip radius, which provides measurements at larger loads and penetration depths. At small penetration depth, the measurement is affected by surface roughness, while at large penetration depths the measurement is affected by the presence of the much softer molybdenum substrate. Thus, the peaks in the curves seen in Fig. 33 are representative of the films "true" hardness. The measured hardness values were significantly higher for the film deposited at 700 °C than for the lower-temperature film, reaching a peak of over 37 GPa, above the range of values reported for standard bulk silicon carbide. We expect that the density and hardness can be further improved by appropriate film post processing techniques.

References

1. J. Fernandez de la Mora, S.V. Hering, N.P. Rao, and P.H. McMurry: *J. Aerosol Sci.*, 1990, vol. 21 (2), pp. 169-87.
2. N.P. Rao, H.J. Lee, M. Kelkar, D.J. Hansen, J.V.R. Heberlein, P.H. McMurry, and S.L. Girshick: *Nanostruct. Mater.*, 1997, vol. 9, pp. 129-32.
3. N P. Rao, N. Tymiak, J. Blum, A. Neuman, H.J. Lee, S.L. Girshick, P.H. McMurry, and J. Heberlein: *J. Aerosol Sci.*, 1998, vol. 29 (5-6), pp. 707-20.
4. J. Blum, N. Tymiak, A. Neuman, Z. Wong, N.P. Rao, S.L. Girshick, W.W. Gerberich, P.H. McMurry, and J.V.R. Heberlein: *J. Nanoparticle Res.*, 1999, vol. 1 (1), pp. 31-42.

32. Comparison of the Microstructure of Perovskite Coatings Synthesized by Suspension Plasma Spraying and TPCVD

M. Müller, E. Bouyer, M. von Bradke, R. Henne, and G. Schiller
Deutsches Zentrum für Luft- und Raumfahrt (DLR) Institut für Technische Thermodynamik, D-70569 Stuttgart, Germany

Introduction

Fuel cells are highly efficient converters of chemical into electrical energy.[1] In solid oxide fuel cells (SOFCs), the components of the membrane electrode assembly (MEA) consist of either oxide ceramics or cermets. Different techniques are being applied for the manufacture of the three layer MEAs, such as tape casting and sintering. Successful application of vacuum plasma spraying was also described by several research groups.[2–5]

While the electrolyte of the fuel cell must be gas-tight and hence of only little and closed porosity, the electrodes must ensure an appropriate gas flow to an as large as possible three phase boundary layer between electrolyte, electrode, and reaction gas. Therefore, an open porous electrode structure must be established. This can hardly be attained by traditional plasma spray methods yielding a pancake-like coating texture. One solution was proposed by Tai *et al.* who co-processed perovskite and carbon additives.[3] In this study, attempts to deposit porous SOFC cathode layers by means of suspension plasma spraying (SPS) and TPCVD are compared. The procedures are explained in detail elsewhere.[6,7] The SPS related part of this work has been published in Ref 8.

Experimental Procedure

The plasma was generated using a PL50 Plasma Torch from TEKNA which was mounted on a vacuum reactor. The SPS experiments were performed with a two phase feedstock of MnO_2 powder suspended in a saturated solution of $LaCl_3$ in ethanol. The TPCVD experiments were performed with an aqueous solution of lanthanum and strontium nitrates and manganese acetate. The molar ratio (La,Sr):Mn was always 1. During some experiments, different amounts of oxygen were added to the plasma sheath gas.

Results and Discussion

The SPS synthesized coatings have the typical lamellar microstructure of plasma sprayed coatings. This reveals the deposition of molten droplets as can be expected from the suspension feedstock. The porosity is low and there are no open pore channels from the bottom to the top of the coating (Fig. 34); hence, a

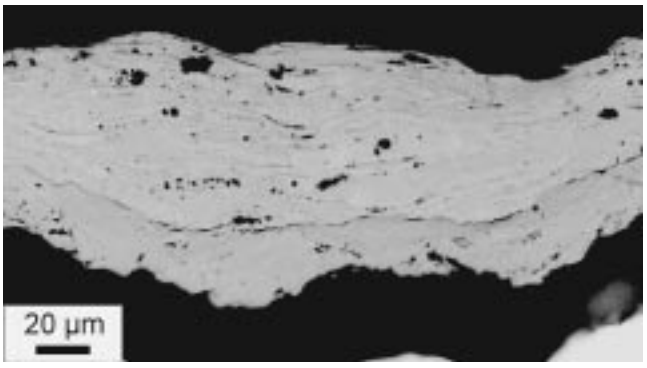

Fig. 34 Optical micrograph of a cross section of a suspension plasma sprayed perovskite coating

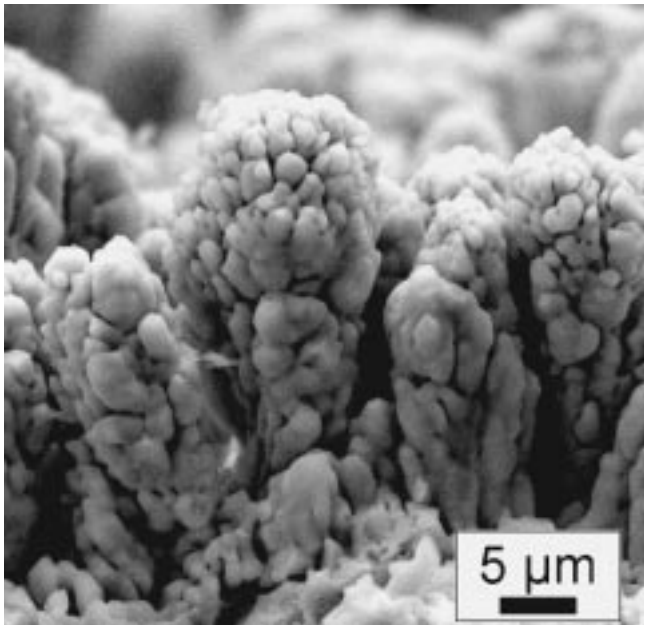

(a)

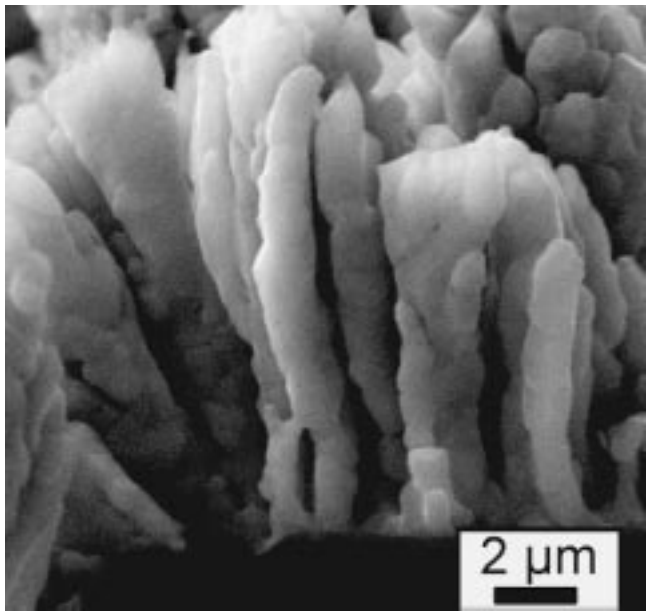

(b)

Fig. 35 SEM images of fracture sections of TPCVD perovskite coating

poor capability of gas transport in the fuel cell application is the result. The growth rate of the coating exceeds 100 μm/min.

The TPCVD synthesized coatings show a cauliflower-like or even columnar growth (Fig. 35). Obviously no impinging droplets of in-flight formed particles built up the coating, but radicals and clusters corrected to become more clean form a coating under certain plasma and injection conditions. As a result, beneficial open porosity could be achieved. The growth rate of the coating was about 30 μm/min.

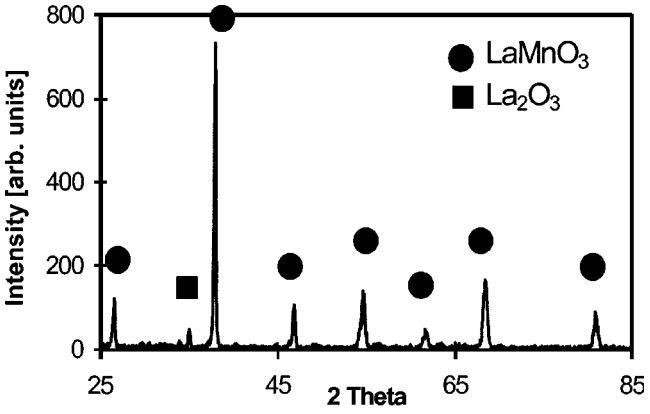

Fig. 36 X-ray diffraction pattern of a TPCVD perovskite coating

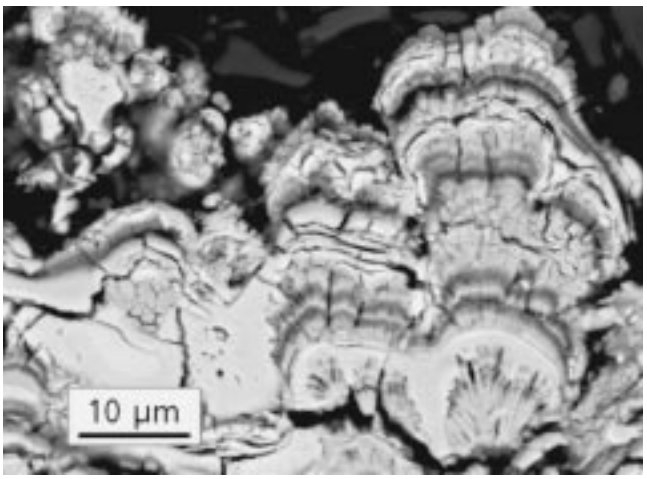

Fig. 37 SEM image (backscattered electrons) of a cross section of a TPCVD perovskite coating

The phase content of the SPS synthesized coatings was mainly $LaMnO_3$ (perovskite), Mn_3O_4 , and La_2O_3. The highest purity of the perovskite phase was obtained in the center of a stationary sample; *i.e.*, in the plasma jet axis. In contrast, the TPCVD synthesized coatings exhibited the highest amount of detrimental free La_2O_3 in the center of the stationary sample, while almost pure and well crystallized perovskite phase was formed in the outer regions (Fig. 36). The nucleation of the single phases and hence the "fixing" of the chemical elements start at different temperatures and, hence, at different radial distances from the plasma jet axis. This can be emphasized with the observation of the element distribution within a sample that was scanned in the *x-y* direction in the plasma jet. The single cauliflower-like aggregates of the coating show a zonar growth with alternating La-Sr-richer zones (Fig. 37, bright) which can be assigned to the free La-Sr-oxides, zones of less La-Sr-content to be assigned to the requested perovskite phase and carbon-rich phases (from acetate, Fig. 37, dark). Generally, a homogeneous co-existence of lanthanum and strontium can be observed. The uniform Sr-doping is the precondition for the requested conduction and heat expansion properties of the perovskite SOFC cathode.

Conclusions and Outlook

The TPCVD process seems to offer the greater variability with respect to the control of the coating microstructure compared to the SPS process. Applying the SPS process can achieve higher growth rates. A problem to be solved is the impurity of the coatings. A homogeneous Sr-doping was achieved; however, undesired phases such as free (La,Sr)-oxides occur which may hydrate and hence mechanically destroy the coating. The stoichiometry of the precursors must be adapted to avoid this drawback.

References

1. N.Q. Minh and T. Takahashi: *Science and Technology of Ceramic Fuel Cells*, Elsevier, Amsterdam, (1995).
2. T. Yoshida, T. Okada, H. Hamatani, and H. Kumaoka: *Plasma Sources Sci. Technol.*, 1992, vol. 1, pp. 195-201.
3. L.-W. Tai and P.A. Lessing: *J. Am. Ceram. Soc.*, 1991, vol. 74 (3), pp. 501-04.
4. R. Henne, G. Schiller, V. Borck, M. Müller, M. Lang, and R. Rückdäschel: in *Thermal Spray: Meeting the Challenges of the 21st Century*, C. Coddet, (ed.), ASM International, Materials Park, OH, 1998, pp. 933-38.
5. H. Gruner and H. Tannenberger: *Proc. 1st Eur. SOFC Forum*, Lucerne, Switzerland, 1994, vol. 2, pp. 611-17.
6. F. Gitzhofer, E. Bouyer, and M.I. Boulos: U.S. Patent No. 5,609,921, 1997.
7. H. Zhu, Y.C. Lau, and E. Pfender: *J. Appl. Phys.*, 1991, vol. 69 (5), pp. 3404-06.
8. G. Schiller, M. Müller, and F. Gitzhofer: in *Thermal Spray: Meeting the Challenges of the 21st Century*, C. Coddet, ed., ASM International, Materials Park, OH, 1998, pp. 363-67.

33. Twin Wire Arc and High Energy Plasma Spray Coating Using Nanometer Scale WC-Co in Powder-Filled Cored Wire

D.G. Atteridge, R. Davis, M Scholl, and G. Tewksbury
Oregon Graduate Institute of Science and Technology, Portland, OR

M. Becker
Portland State University, Portland, OR, and Knolls Atomic Power Laboratory, Schenectady, NY

R. Travis and J. Herbstritt Puget
Sound Naval Shipyard, Bremerton, Washington

Introduction

It is desired to assess the use of nanometer scale tungsten carbide (WC) particles in thermal spray applications. The thermal spray techniques used in this study were twin-wire-arc-spray (TWAS) and high-energy-plasma-spray (HEPS). Powder filled wire was used as the feedstock for this assessment, as it is required for TWAS application. The use of a powder-filled wire also allows use of WC-containing powders that are difficult and/or impossible to feed into thermal spray units, such as HEPS or high-velocity-oxyfuel, using standard powder feed techniques. The powder used in this study was found to be difficult to feed and exhibited a low coating capture efficiency in HEPS applications due to its high volume of fines mixed with large particles. The nanometer scale WC particles used in this study were embedded in a cobalt matrix and were produced as a multiparticle agglomerate. The WC-Co powder feed was produced by Nanodyne Inc. using a spray conversion process.

The data currently reported is part of a larger program examining the potential of these materials as feedstock for thermally sprayed coatings. HEPS was examined due to its ability to spray many forms of feedstock, both in type and size, while producing high quality coatings. TWAS was used since it can reach deposition rates and efficiencies which far exceed those of other processes, as well as being the preferred thermal spray technique for large-area applications.

Materials and Processes

Thermally sprayed coatings were made using tungsten carbide-cobalt (WC-Co) powder-filled cored wire made from powders with nanometer scale tungsten carbide (WC) grains. Three different cored wires were produced by Devasco using two different wire sheath materials. The sheath materials were nickel and 430 stainless steel and were filled with either 6 or 15 wt.% Co (remainder is nanometer scale WC) WC-Co powders. Both 6 and 15 wt.% WC-Co powders were used with the Ni sheathed wire (denoted Ni-WC6Co and Ni-WC15Co, respectively), while only the 6 wt.% WC-Co was used with the 430 stainless steel sheath material (denoted 430SS-WC6Co). The cored wire diameter (3/32 in.) and sheath thickness (0.012 in.) combined to yield a sheath-to-powder volume ratio of one to one (1:1). The cored wires were used as feedstock for producing coatings using twin wire arc spray and high energy plasma spray. The WC coating content was estimated to be nominally 25 wt.% WC for the 15% Co powder cored wire and 30 wt.% WC for the 6% Co powder cored wire, when the volume of sheath and Co material as well as the original powder porosity and powder packing efficiency were taken into account.

Twin wire arc spraying feasibility for the nano-WC-Co cored-wire feedstocks was carried out at the Puget Sound Naval Shipyard (PSNS) using a Thermion system. Air pressure was held constant at 100 psi while current was held constant at 200

amps. Initial voltage settings were determined using a Devasco-produced high-manganese cored-wire due to the small quantities of the wire containing the nanometer scale WC. This technique conserved substantial amounts of wire. The experimental spray parameters varied from 25 to 35 Volts, but were not optimized due to the small quantity of material available. The core wire was found to be sprayable at lower voltages than solid wire feedstock, and that none of the cored wires contained fluxing agents as found in cored welding wire.

The high energy plasma spraying was carried out at the Oregon Graduate Institute using a 200 kW Plazjet plasma spraying system. This system operates from 200 to 500 V and 100 to 500 amps, with gas flows from 100 slpm nitrogen to over 400 slpm nitrogen. Nitrogen/hydrogen mixtures can also be used at ratios over 1:1. The system is capable of spraying both wire feedstock from 0.035 to 0.125 in. in diameter or powder feedstock from 10 to over 150 m in size; or both may be used simultaneously. As with the TWAS, parameters were assessed with the high-manganese cored wire before using the nanometer scale WC-containing wire. Nominal spraying parameters were 5 cfm nitrogen, up to 2 cfm hydrogen, 400 V, and 400 amps, and resulted in a 0.030 in. thick coating.

All three wires (Ni-WC6Co, Ni-WC15Co, and 430SS-WC6Co) were used to produce coatings with the TWAS system, while only the nickel-sheathed wires were used to produce coatings with the HEPS system (Ni-WC6Co and Ni-WC15Co). Coatings were deposited on carbon steel substrates grit-blasted immediately prior to spraying. Several spray parameter sets were run for each thermal spray technique, although parameter optimization was not possible due to the limited amount of cored wire procured for this feasibility study. Coating thickness of nominally 1 mm was achieved using TWAS with no spalling of the coating. Subsequent analysis and testing included optical microscopy, scanning electron microscopy, transmission electron microscopy, dry-sand, rubber-wheel wear testing, bend testing, and adhesion strength testing.

Coating Properties

Wear resistance was found to improve with increasing WC content and with increasing voltage. The 430SS-WC6Co coating wear rate was superior to that of the nickel-based coating. Adhesion strength was also found to improve with increasing WC content. Twin wire arc coating adhesion values were found to be very high. The adhesion values for the nickel-sheathed twin wire arc coatings were found to be 9.2 ksi for the 15% Co coating and 10.4 ksi with the 6% Co coatings, with the latter values being a lower bound as the test failures took place in the epoxy versus the coating/interface. In fact, the Ni-WC6Co twin wire arc coating adhesion results were found to be the highest thermal spray coating adhesion results to date by the Puget Sound Naval Shipyard. The 430SS-WC6Co coating exhibited an adhesion strength of 7.6 ksi. All coatings passed the bend test.

Optical microscopy and SEM analysis showed porosity values for the TWAS coatings to be about 3% for the nickel-based coatings and 7% for the 430 stainless steel coatings. The porosity of the HEPS nickel-based coatings was found to be higher than that of the TWAS nickel-based coatings. Backscattered imaging in the SEM also revealed that the distribution of the WC-Co was non-uniform in the as-sprayed deposit. This indicates that portions of the original WC-Co powder did not mix uniformly with the sheath material.

The cored-wire feedstock was readily sprayed by both TWAS and HEPS. The nanoscale WC increased wear and adhesion strength despite not having a high WC volume fraction. The nano-WC-Co cored-wire filler powder was (partially) integrally mixed into the sheath material.

34. Thermal Spray of Nanostructured Alumina/Titania Feedstock for Improved Properties

T.D. Xiao, S. Jiang, Y. Wang, D.M. Wang, and P.R. Strutt
Inframat Corporation, Willington, CT 06279

Individual nanoparticles cannot be successfully thermal sprayed because of their low mass and their inability to be carried in a moving gas stream and deposited on a substrate. To overcome this, Inframat staff have developed a patent pending process to reconstitute individual nanoparticles into spherical micron-size granules that can be thermal sprayed.[1-3] The developed methodology involves the dispersion of nanopowders into a colloidal suspension, followed by the addition of a binder and subsequent spray drying into granules. The methodology is very general in nature and has been used to make sprayable granules from metal, ceramics, and composite nanopowders. The obtained nanocoatings are dense and possess improved mechanical properties. Here, we report the reconstitution and thermal spray of the nanostructured alumina/titania (n-Al_2O_3/TiO_2).

Reconstitution

The reconstitution of nanostructured materials is a very important step in determining the powder feed characteristics and coating performance. The powder feeding of nanostructured materials is directly related to the feedstock morphology and particle size. The ideal powder feedstocks should have a spherical morphology, dense particles, and a narrow particle size distribution to ensure good flowability in the existing powder feeding systems.

Thermal Spray

The reconstituted n-Al_2O_3/13TiO_2 (13 wt.% TiO_2) feedstock has also been thermal sprayed using the Metco 9MB gun system.

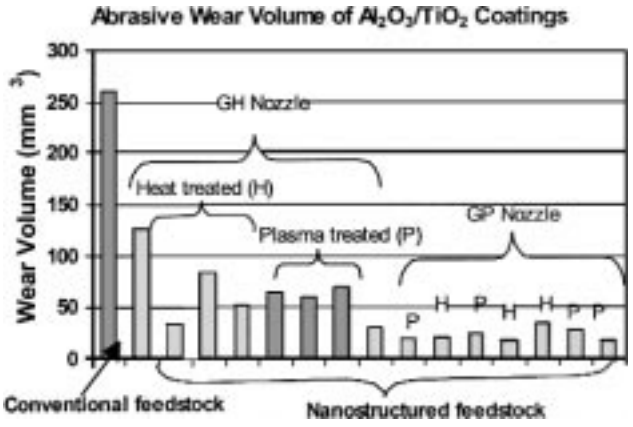

Fig. 38 Wear property comparisons, nanostrucured Al_2O_3/TiO_2 vs conventional Al_2O_3

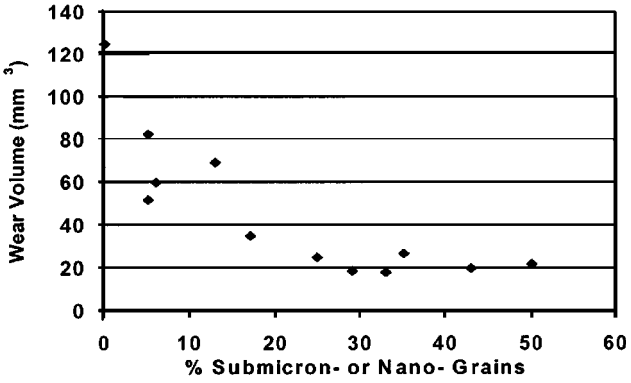

Fig. 39 Plot of wear resistance vs percent of nano- or submicron structure

During plasma spray, it has been demonstrated that the quality of a nanostructured coating is controlled by thermal spray processing parameters. Initial SEM studies indicated that the surface morphologies and densities of conventional and nanostructured $Al_2O_3/13TiO_2$ coatings seemed to be similar at low magnifications. Detailed SEM studies, however, indicated that there is a significant microstructural difference between these coatings. In the nanostructured coating, it seems that the individual grains (Al_2O_3 phase) are well-wetted with the matrix materials (TiO_2 phase), while the conventional coating is not. Further transmission electron microscopy is needed to investigate the detailed microstructure of these coatings in order to understand wear mechanisms of these two materials. It should be emphasized that the average particle size of both conventional and *n*-$Al_2O_3/13TiO_2$ are ~40 μm. Each agglomerate of the commercial $Al_2O_3/13TiO_2$ feedstock contains only a few micron-sized grains, while the *n*-$Al_2O_3/13TiO_2$ agglomerated particle is an assemblage of many nanometer-sized grains.

Mechanical Properties

The abrasive wear tests were performed on a grinding/polishing machine at room temperature. Prior to the wear tests, coating surfaces were polished to 1 μm after 9 and 3 µm polishing steps, and then cleaned with acetone. The tests were conducted under the normal load of 45 N. Coated samples were used as pins (cylindrical samples) with a flat surface of 32 mm in diameter. A 40 µm diamond abrasive pad with diameter of 170 mm was used as the disk. It was dressed and cleaned before each experiment and lubricated with water during the tests.

The wear volumes of different Al_2O_3/TiO_2 coatings are presented in Fig. 38. The conventional coating has the lowest wear resistance. The wear resistance of the coatings sprayed with heat-treated *n*-Al_2O_3/TiO_2 powder is about 2 times that of a coating sprayed using conventional powder. The plasma treated *n*-Al_2O_3/TiO_2 exhibits ~4 times increase in wear resistance. It should be noted that the wear resistance of *n*-Al_2O_3/TiO_2 coatings is remarkably improved by using the GP nozzle. The wear resistance of the *n*-Al_2O_3/TiO_2 coating sprayed with both the heat-treated and plasma-processed feedstock was more than 8 times improved over the commercial Al_2O_3/TiO_2 when a GP nozzle was employed.

The microstructure of ceramics, especially grain size, has an immense influence on the wear resistance. Figure 39 shows the relationship between the percentage of submicro- or nanostructured grains and the wear volume of Al_2O_3/TiO_2 coatings. The coatings with higher percentage of submicro- or nanostructured grains exhibited excellent wear resistance. It should be emphasized here that the percentage of submicro- or nanostructured coatings is increased by using a GP nozzle.

In summary, nanostructured powders have been successfully reconstituted into thermally sprayable feedstocks. This is a generic process, which is applicable to reprocess nanostructured metals, ceramics, and their composites. The reconstituted nanopowder feedstocks have also been thermally sprayed into coatings. Microstructural characterization revealed that the morphological features of the as-produced nanocoatings are dense. The hardness of the *n*-Al_2O_3/TiO_2 is similar to the commercial Al_2O_3/TiO_2 with the same composition. Preliminary wear data have indicated that *n*-Al_2O_3/13 wt.% TiO_2 coatings have better wear performance.

Acknowledgments

The authors would like to thank the Office of Naval Research for providing financial support under Contract Nos. N00014-97-1-0843 (ONR Contract, UConn/Inframat) and N00014-98-30005 (ONR DUST). We are also grateful to Professor Maurice Gell, of the University of Connecticut (UConn), for helpful discussions and management of the coating program. We also thank Professor Leon Shaw, of UConn, for technical discussions.

References

1. P.R. Strutt, B.H. Kear, and R.F. Boland: U.S. Patent 6,025,034, Feb. 15, 2000, original application filed Nov. 1995 and abandoned.
2. T.D. Xiao, C.W. Strock, D.M. Wang, and P.R. Strutt:, U.S. Patent filed Aug. 1997.
3. B.H. Kear and P.R. Strutt: *Naval Rev.* 1994, vol. XLVI, p. 4.

35. Properties and Microstructures of Nanostructured Alumina-13% Titania + Zirconia Coatings

R.S. Lima, A. Kucuk, U. Senturk, and C.C. Berndt
Department of Materials Science and Engineering State University of New York at Stony Brook, Stony Brook, NY 11794-2275

Alumina-titania-zirconia coatings have potential for applications that require wear resistance at low temperatures. Although alumina coatings with their high hardness may be used in wear resistance applications, the low toughness of alumina coatings limits their use. It was reported that titania or zirconia additions to alumina increases the fracture toughness of the coatings. Barbezat *et al.*[1] measured Vickers hardnesses of 825 and 1100 kgf/mm^2 for atmosphere plasma sprayed Al_2O_3-40ZrO_2 and Al_2O_3-13TiO_2 coatings, respectively. It was also reported that the fracture toughness of the Al_2O_3-13TiO_2 coating, 3.8 MPa.m$^{1/2}$, is higher than that of an Al_2O_3 coating, 2.8 MPa.m$^{1/2}$. Takeuchi *et al.*[2] measured microhardness of atmosphere plasma sprayed alumina and alumina-titania coatings as 720 and 690 kgf/mm^2, respectively. Stevens[3] reported that alumina-zirconia coatings have higher toughness than alumina coatings due to a transformation toughening effect, while these two coating systems have similar hardness values.

Nanostructured materials have gained special interest due to their superior properties with respect to their microstructured counterparts. In the current study, nanosize alumina-titania-zirconia (ATZ) was atmosphere plasma sprayed to examine the potential use of this nanosized material as a coating.

ATZ coatings of 0.7 to 1 mm thickness on mild steel substrates were produced using a Miller SG100 commercially available plasma-spray gun with the processing conditions listed in Table 5. ATZ coatings in the as-sprayed condition exhibited a dark blue appearance. Figure 40 illustrates a typical x-ray diffraction pattern for an ATZ coating. As shown, the coating is a mixture of α-Al_2O_3, t'-ZrO_2, γ-Al_2O_3, β-Al_2TiO_5, and an unknown phases.

Microhardness of the coatings was measured using a Vickers microhardness tester on polished top and cross section surfaces with 500 and 1000 g loads (Figs. 41 and 42). As given in Fig. 41, there is no significant difference in the hardness values measured on the cross section and the top surfaces using either 500 or 1000 g. In addition, the hardnesses of the coatings sprayed with 40 kW power at 60 and 80 mm are statistically the same, whereas coat-

Table 5. Spray parameters

Parameters	ATZ-1	ATZ-2	ATZ-3	ATZ-4	ATZ-5
Voltage (V)	50	50	50	40	40
Current (A)	800	800	800	800	600
Power (kW)	40	40	40	32	24
Primary gas (Ar) 48 flow (slpm)	48	48	48	48	
Secondary gas (H_2) flow (slpm)	~3	~3	~3	~1	~1
Spray distance (mm)	60	80	100	60	60

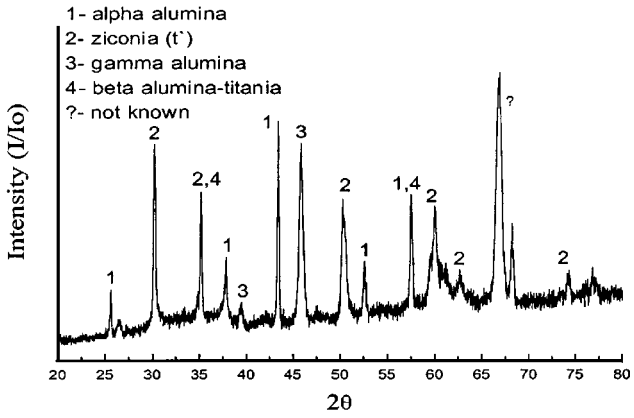

Fig. 40 X-ray diffraction analysis of alumina-titania coatings

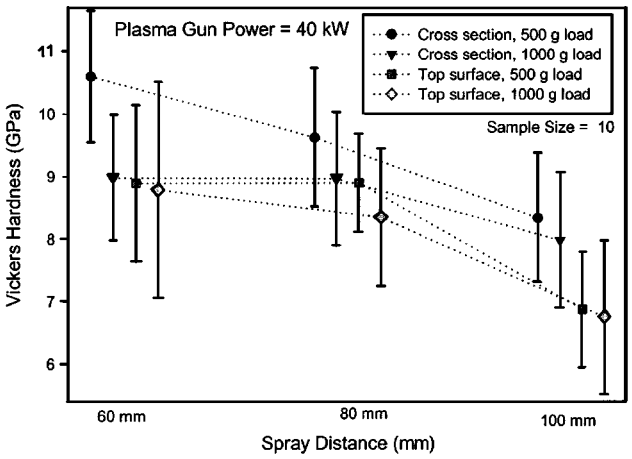

Fig. 41 Change of microhardness of ATZ coating sprayed at different standoff distances

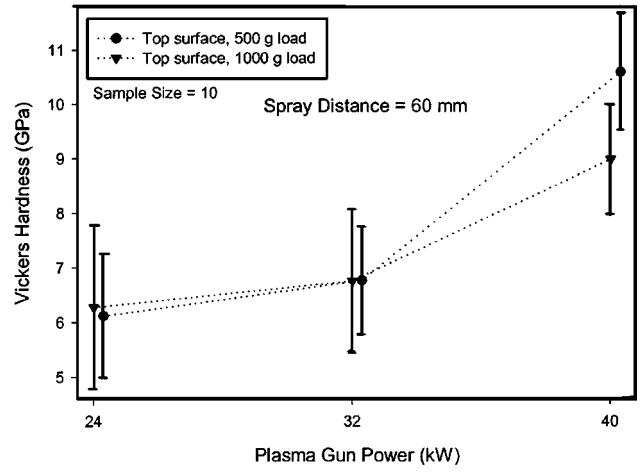

Fig. 42 Change of microhardness of ATZ coatings sprayed using different plasma powers at a 60 mm standoff distance

ings sprayed at a 100 mm standoff distance have lower hardness than those sprayed at 60 and 80 mm.

The hardness of ATZ coatings sprayed using different plasma gun powers at a 60 mm standoff distance is illustrated in Fig. 42. The hardness of ATZ coatings sprayed using 24 and 32 kW powers are statistically the same, while the coatings sprayed using 40 kW exhibit significantly higher microhardness values than those of the aforementioned materials. It is believed that higher power and shorter spray distance result in splats with higher temperature and, therefore, more effective packing in the deposit. This more effective packing provides an increase in the hardness measurement of the coatings.

In the current study, it was shown that a commercially available torch could be used to spray nanosized alumina-titania-zirconia. It was also found that the properties of coatings depend on the spray parameters. Spray parameters to produce coatings with improved characteristics were developed. Coatings sprayed at higher powers and lower spray distances were found to have higher microhardness. It was found from x-ray diffraction analysis that coatings contain a mixture of α-Al_2O_3, t'-ZrO_2, γ-Al_2O_3, β-Al_2TiO_5, and an unknown phases.

Acknowledgements

This work is supported under ONR Grant No. N00014-97-0843 and under NSF-MRSEC DMR Grant No. 9632570.

References

1. G. Barbezat, A. Nicoll, and A. Sickinger: *Wear*, 1993, vol. 162-164, pp. 529-37.
2. J. Takeuchi, H. Nakahira, and J. Nagai: *2nd Plasma Technik Symp.*, Lucerne, Switzerland, 1991, pp. 141-51
3. R. Stevens: *Zirconia and Zirconia Ceramics*, Pub. Magnesium Elektron, Twickenham, United Kingdom, 1986.

36. Synthesis and Characterization of Cryomilled SiC Reinforced Al Coatings

M. Ice, R. Rodriguez, D. Cheng, and E. J. Lavernia
Department of Chemical and Biochemical Engineering and Materials Science and University of California, Irvine, CA 92697-2575

G. Kim
PyroGenesis Inc., Montreal, PQ, Canada H3J 1R4

M. Trudeau
Technologies Emergentes IREQ, Hydro-Quebec, Lionel-Boulet, PQ, Canada J3X 1S1

J. Terlecki
Applied Analytical Sciences, Costa Mesa, CA 92626

The combination of modern processing techniques may be implemented to improve the properties of nanostructured materials. Two such processes, cryomilling and thermal spraying, were the key manufacturing tools for the research presented here. In this study, commercial 3003 Al alloy powder was blended with 10 vol.% SiC powder and mechanically milled under liquid nitrogen to produce a metal matrix composite with a nanocrystalline microstructure. Subsequently, these powders were thermally sprayed onto a mild steel substrate by plasma spraying to produce a metal-matrix composite (MMC) coating. X-ray diffraction, scanning electron microscopy with energy dispersive spectroscopy, and acid dissolution were used to characterize the cryomilled powders and the coatings. Mechanical tests include hardness and adhesion.

X-ray analysis shows the grain size prior to plasma spraying to be about 24 ± 50 nm. Nanoindentations performed on the coatings show that the hardness of the SiC reinforced thermal sprayed coating is higher than that of coatings produced from unreinforced powders. Adhesion tests show that both types of coatings have bond strengths higher than that of the epoxy used to conduct ASTM testing.

Index of Authors

All authors of all the abstracts are indexed. The numbers refer to the abstract number.

Alphabetical listing of abstract titles with the primary author and abstract number.